

17. DATA REPORT: PHYSICAL PROPERTIES RELEVANT TO SEISMIC STRATIGRAPHIC STUDIES, CONTINENTAL RISE SITES 1095, 1096, AND 1101, ODP LEG 178, ANTARCTIC PENINSULA¹

V. Volpi,² A. Camerlenghi,² T. Moerz,³ P. Corubolo,² M. Rebesco,²
and U. Tinivella²

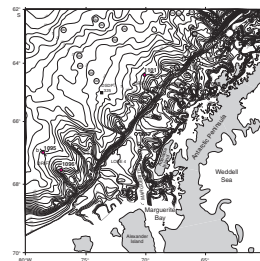
INTRODUCTION

We have reanalyzed the porosity, bulk density, and seismic velocity information collected from continental rise Sites 1095, 1096, and 1101 during the drilling of Ocean Drilling Program (ODP) Leg 178 (Fig. F1). The purpose is to provide a comprehensive composite digital set of data readily available for future studies aimed at well-seismic correlation. The work originates from the occurrence of overlapping sets of physical parameters and acoustic velocity collected by different methods (down-hole logging, core logging, laboratory determination, and derivation from seismic data) and from different holes at the same site. These data do not always provide the same information because of difficulties encountered at each specific hole or methodological differences. In addition, a basic correlation between these parameters and onsite multichannel seismic (MCS) data is presented.

METHODS

To avoid unnecessary duplication of text, we do not include in this paper detailed descriptions of the methods used to derive the physical parameters on board the *JOIDES Resolution*. We refer the reader to the

F1. Location map of sites drilled during Leg 178, p. 11.



¹Volpi, V., Camerlenghi, A., Moerz, T., Corubolo, P., Rebesco, M., and Tinivella, U., 2001. Data report: Physical properties relevant to seismic stratigraphic studies, continental rise Sites 1095, 1096, and 1101, ODP Leg 178, Antarctic Peninsula. *In* Barker, P.F., Camerlenghi, A., Acton, G.D., and Ramsay, A.T.S. (Eds.), *Proc. ODP, Sci. Results*, 178, 1–36 [Online]. Available from World Wide Web: <http://www-odp.tamu.edu/publications/178_SR/VOLUME/CHAPTERS/SR178_17.PDF>. [Cited YYYY-MM-DD]

²Istituto Nazionale di Oceanografia e di Geofisica Sperimentale–OGS, Borgo Grotta Gigante, 42/c I-34010 Sgonico (Trieste) Italy. Correspondence author: vvolpi@ogs.trieste.it

³GEOMAR Research Center for Marine Geoscience, Wischhofstrasse 1-3, D-24148 Kiel, Federal Republic of Germany.

Initial receipt: 2 January 2001

Acceptance: 14 June 2001

Web publication: 14 September 2001

Ms 178SR-228

appropriate chapter of the Leg 178 *Initial Reports* volume (Shipboard Scientific Party, 1999a).

Depth Scale

All data are presented in meters below seafloor (mbsf) vertical scale. We decided to maintain this vertical scale for the following reasons:

1. Two meters-corrected depth scales have been generated for Sites 1095 and 1096—one was generated on board and was included in the *Initial Reports* volume, although it was not included in the Janus database (see “Composite Depths” sections in the site chapters of Shipboard Scientific Party, 1999b, 1999c). Subsequently, another corrected scale was proposed by Barker (Chap. 6, this volume) and was added to the Janus database. At the moment, we are not able to find criteria helpful to select one as the best.
2. For the purpose of this paper, the small vertical shifts (a few meters at most) imposed by the composite depth scale do not significantly affect the results.
3. By presenting the data vs. the original mbsf scale, we allow any user to apply his/her own preferred depth correction, if needed.

Core Logging and Core Sample Data

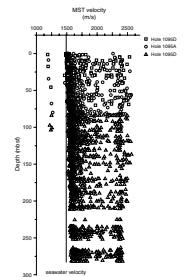
Multisensor Track Velocity

The output files from the multisensor track (MST) instrument typically contain errors resulting from velocity values that are unrealistically low (~1200 m/s), produced by voids in cores, or excessively high, resulting from the presence of dropstones in cores and core section edge effects (Fig. F2). To systematically clean the data, we manually removed the unrealistically low values and averaged the values at 3.5-m intervals. This interval spacing was selected to scale the measurements to a resolution that is appropriate to the available seismic reflection data, considering the nominal vertical resolution of seismic reflection data is equal to one-quarter of a wavelength (λ). Assuming that the generator injector (GI)-gun survey preserves a frequency of 130 Hz, $\lambda/4$ is 3.5 m for a formation velocity of 1800 m/s. In the process of averaging within each 3.5-m interval, the standard deviation is calculated and data points generating a standard deviation in excess of a certain value are excluded from the computation. The process of determining the discriminating standard deviation is iterative and is conducted with a critical eye by the operator. In our case, we decided to keep all values within eight standard deviations to reject only the values that have a very low possibility of belonging to the considered distribution.

Multisensor Track Density and Porosity

Bulk density is calculated as a function of gamma ray attenuation. Porosity is calculated assuming a constant specific gravity of the solid part, knowing the water content of the sediments. The dispersion of these data is much less pronounced than that of the MST velocity data. A procedure analogous to that applied for velocity data was applied to bulk density and porosity.

F2. Sonic velocity raw data output from the MST core logger, p. 12.



Hamilton Frame Velocity

This measurement is conducted manually by an operator who selects appropriate parts of the core. Data can be obtained with two transducers inserted as a fork in the soft sediment in two orthogonal directions (PWS1 and PWS2) or by using a pair of cylindrical transducers (PWS3) that are analogous to those mounted on the MST. To preserve homogeneity of the data, we used PWS3 data, complemented by MST data where possible. With the exception of evident errors, the data were used without any correction of the original file. Errors in the Site 1095 PWS3 data set included in the Leg 178 *Initial Reports* volume were identified between 56.522 and 82.523 mbsf and between 359.343 and 414.844 mbsf (Fig. F3). Velocity in these intervals is shifted systematically toward higher values because a problem occurred during acquisition. The error was identified on board and a correction was applied before generation of the plots presented in the *Initial Reports* volume. The data included in this paper are corrected.

Laboratory Density and Porosity

Porosity and bulk density were obtained as part of the index properties (IP) measurements in the laboratory. Because these measurements were conducted on discrete samples carefully selected by the operator, with a spacing that was usually every core section (1.5 m) and therefore well within the limit of 3.5 m selected as appropriate to the resolution of the seismic profiles, we decided to use these data preferentially with respect to MST data. With the exception of evident errors, the data were used without any correction of the original file.

Final Treatment Common to All Data Sets

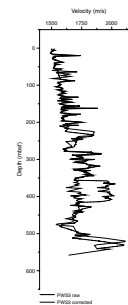
Vertical profiles of velocity, density, and porosity derived from core logs or core samples were obtained by combining data from different instruments and different holes aiming at reconstructing composite profiles for each parameter at each site (Table T1). Finally, all the composite files were gently smoothed and resampled every 2 m after linear interpolation between data points.

Downhole Logging Data

Following the suggestions contained in pertinent sections of the *Initial Reports* volume (Shipboard Scientific Party, 1999b, 1999c), we utilized RHOM (lithodensity sonde [LDS] corrected) bulk density values and porosity values from the APLC (accelerator porosity sonde [APS] near-array limestone porosity corrected) files. No further correction was applied to the data. Sites 1095 and 1096 do not provide velocity information from sonic logs. Site 1101 was not logged at all. For evaluation of the quality of the data, we also used caliper logs.

To avoid duplication of text readily available in ODP and open literature, we suggest the interested reader consult Shipboard Scientific Party (1999a), Goldberg (1997), and Broglia and Ellis (1990) for an understanding of methods and acronyms used by ODP.

F3. Error in PWS3 data files, Site 1095, p. 13.



T1. Compilation of composite profiles from core data, p. 28.

Vertical Seismic Profile

Only one vertical seismic profile (VSP) was carried out, at Site 1095 (Shipboard Scientific Party, 1999b). The spacing of the recording stations makes this data set more appropriate for a velocity check shot than for the generation of a proper vertical seismic profile. However, both on the ship and in this study, the data were processed to obtain a low-coverage VSP.

The interval velocities obtained on board are considered reliable. They were obtained as a straightforward division of the distance between stations and difference in traveltime. However, the VSP processing was delivered as a closed result, with no possibility of refining the onboard processing. Therefore, we reprocessed the data as follows:

1. Separation of upgoing and downgoing fields using a median filter;
2. Predictive deconvolution of upgoing events using 500-ms operator length and automatic prediction lag. However, because a GI gun was used, deconvolution is not critical;
3. Conversion of the upgoing field to two-way traveltimes (TWT);
4. Corridor stack;
5. Filter for display 12–24/60–80 Hz;
6. Prediction of the depth of the deeper reflector using a plot of TWT vs. depth; and
7. Plot of the interval velocities against stacking velocities at the nearest shotpoint (SP) (1250 m).

A note of caution on the available raw VSP data: the data were transferred via internet from the ODP Borehole Research Group database. We encountered three kinds of problem:

1. Data are in ASCII format rather than SEG-Y standard format. Additional information was added in manually created headers.
2. Traveltimes are neither total traveltimes from the source nor traveltimes from the seafloor. Evidently, the traveltimes were muted with no specification. A comparison with traveltime tables recovered from the shipboard recording and available in the published report allowed us to reduce, by application of a constant shift, the traveltimes of the database to traveltimes from the seafloor. Relative traveltimes were found to be coherent with shipboard data.
3. The total depths used on the ship were relative to the rig floor. In our calculations, we considered depth relative to sea level by subtracting 11 m (the distance of the rig floor from sea level). After this data reduction, we observed that the picking of first arrival is in agreement with that obtained on the ship, with a tolerance of one or two sampling intervals.

Velocity Field from Tomographic Inversion of Traveltimes

A velocity analysis was carried out on MCS profiles at Site 1096 prior to drilling to derive a detailed velocity structure useful to site evaluation and planning of drilling. In addition to the standard stacking velocity evaluation, an inversion of traveltimes of selected reflectors was applied

to a 5-km-long segment of MCS line IT90-109 from SP 1880 to 1980 (centered on Site 1096) using an acoustic tomographic technique.

The reflection tomography algorithm adopted here is described by Carrion et al. (1993a, 1993b), and an example of its application to MCS data from the Antarctic margin is provided by Tinivella et al. (1998). A detailed description of the method is reported also by Tinivella et al. (Chap. 16, this volume). The MCS data were collected in 1990 with the following parameters: the seismic source was a tuned 40-air gun array with a total capacity of 72 L towed 6 m below the sea surface; the 3000-m-long analog streamer had 120 traces, spaced every 25 m; and a 50-m shot interval provided 30-fold coverage.

Ten reflectors were picked from the seafloor to the base of Unit M4, including unit boundaries from M1 to M4 of Rebeco et al. (1997). Traces with the highest coherency of reflectors were found within the shorter offsets. Ten traces were selected for picking, from 932.5 to 1432.5 m from the ship. The picking was done on both common offset (such as that shown in Fig. F4) and common shot gathers. The tomographic inversion was applied to one of every four shots.

Multichannel Seismic Reflection Profiles

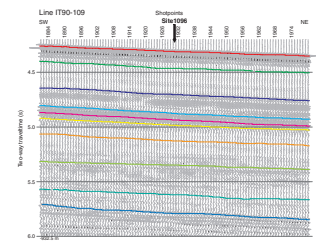
Seismic profiles shown across Sites 1095 and 1096 are the same as those described by the Shipboard Scientific Party (1999a). The two sections presented in this study were produced by rescaling the stack sections, sampling one of every four traces, and displaying the signal as variable density. We do not show MCS profiles across Site 1101 because we have no relevant information to add. We refer to Shipboard Scientific Party (1999d) for seismic displays across this site.

RESULTS

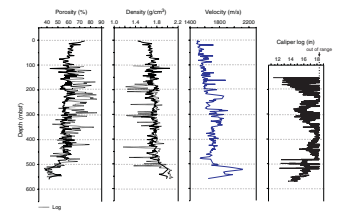
Site 1095

Figure F5, displays the comparison between core sample and downhole log porosity, density, and velocity at Site 1095. With the exception of the lower part of the section (below ~400 mbsf), downhole log porosity is systematically larger than core sample porosity. Excessively high neutron log porosity is normally caused by bound water in clay minerals (Broglia and Ellis, 1990; Goldberg, 1997). However, we used porosity data conventionally corrected for this effect, so that the error induced is surely attenuated, if not eliminated (see “Downhole Measurements” in Shipboard Scientific Party, 1999a). RHOM density, on the other hand, is in fairly good agreement between downhole and core sample data, with the exception of the occurrence of unrealistically low values in the downhole log set, induced by the excessively large size of the hole. This is demonstrated in Figure F5 where a comparison with the caliper log shows that the negative deviations in density occur preferentially when the caliper goes out of range. The effect of hole diameter on the density log is dramatic, whereas it produces a lower effect, but smeared over almost the entire section, on the porosity log. As expected in normally consolidated sediments, porosity decreases downhole, although with variable gradients, from 70%–75% at the sediment surface to ~45% at 550 mbsf. A large reduction in porosity occurs at ~480 mbsf. As expected, the density log obtained from core samples mirrors the porosity

F4. Tomographic inversion of traveltimes, Site 1095, p. 14.



F5. Comparison between downhole and core logging measurements, Site 1095, p. 15.



log, ranging from $\sim 1.6 \text{ g/cm}^3$ at the top (core data) to $\sim 2.1 \text{ g/cm}^3$ at the bottom of the hole.

Figure F5 also illustrates the acoustic velocity values for Site 1095 obtained from core data. Velocity generally increases downhole, from $\sim 1500 \text{ m/s}$ at the top to $\sim 2000 \text{ m/s}$ at the bottom of the hole. There is a fairly steady increase from 0 to 400 mbsf and a sharp increase below 480 mbsf, in parallel with the decreasing porosity and increasing density (see above).

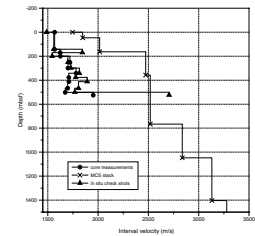
At Site 1095 (Fig. F6), additional information on acoustic velocity comes from the velocity check shots. Eleven interval velocities were calculated, in total agreement with those obtained on board the *JOIDES Resolution* and presented in the Leg 178 *Initial Reports* volume (Shipboard Scientific Party, 1999b). Here, we compare these interval velocities with the nearest available stacking velocities obtained from MCS line 1095 (SP 1210, 1250 m away from the location of Site 1095) and with a reduction to the same intervals of the velocities obtained from core samples. Evidently, the in situ velocity check shots provide more reliable velocity information than the stacking velocity, indicating consistently lower velocity throughout the section. The anomalously high check shot velocity obtained at the base of the hole is interpreted as being produced by an error in the positioning of the geophone. The velocity measured on core samples is consistent with the in situ check shots.

The data plotted in Figure F5 are provided in Table T2.

Site 1096

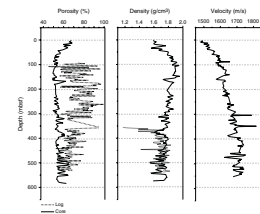
Figure F7 displays the comparison between core sample and downhole porosity, density, and velocity at Site 1096. With the exception of the lowermost part of the section, the porosity distribution with depth varies significantly between the two data sets; downhole logging porosity is systematically higher than core sample porosity. The discrepancy is as large as 25% in the middle part of the section. The downhole log data contain much higher internal variability than the core sample data. According to the core sample data, porosity at the top of the section is in the range of 65%–70%. Downhole log values are not available at the top, but unrealistic values in the range of 70%–80% are present at $\sim 100 \text{ mbsf}$. Both sets converge toward $\sim 60\%$ porosity at the bottom of the hole (580 mbsf). As for neutron porosity data at Site 1095, we think that the clay bound water effect is at least partly attenuated by the standard correction applied to the APLC data set. We consider the data set from downhole logging unrealistic because the logging of Hole 1096 suffered from various problems. Principally, the hole was unstable and large cavities were encountered. Secondly, and more importantly, there was a problem in the range calibration of the caliper so that the hole diameter values used in the correction of the data were probably too small (see “Downhole Measurements” in Shipboard Scientific Party, 1999a). A characteristic of the porosity variation with depth at Site 1096 is that there is a porosity reduction in the uppermost 100 mbsf followed by a slight increase downhole. As a consequence, the lowest porosity values ($\sim 50\%$) are found at 100–150 mbsf. We think that this anomalous trend is real because it is preserved even if the effect of rebound after sampling (normally 2%–3% in this range of overburden pressure, according to Hamilton [1976]) is considered. The density distribution with depth is consistent with the porosity trend. Core sample density increases from $\sim 1.6 \text{ g/cm}^3$ at the surface to $\sim 1.9 \text{ g/cm}^3$ at 100–150 mbsf, decreasing steadily downward to 1.7 g/cm^3 at the bottom of

F6. Comparison among interval velocities, Site 1095, p. 16.



T2. Porosity, density, and velocity, Site 1095, p. 29.

F7. Comparison between downhole and core logging measurements, Site 1096, p. 17.



the hole. The downhole logging data are limited to the lower part of the hole and are in fairly good agreement with the core sample data. Such anomalous behavior of bulk density and porosity at Site 1096 can be explained by the relatively high sedimentation rate (up to 18 cm/k.y.) or by the presence of a large component of biogenic silica (diatom and radiolarian skeletons) throughout the section (Shipboard Scientific Party, 1999c).

Figure F7 also illustrates acoustic velocity values for Site 1096, obtained from core data. Velocity increases rather steadily downhole, with narrow positive and negative excursions from the general trend. The highest gradient is in the upper 100 mbsf, a smaller gradient between 100 and 480 mbsf, and almost no gradient below 480 mbsf. Values range from ~1500 m/s at the sediment surface to ~1700 m/s at the bottom of the hole.

At Site 1096, additional velocity information comes from the acoustic tomographic inversion of traveltimes. Figure F8 shows the distribution with depth of the interval velocity along MCS profile IT90–109. Note that the section is plotted with a vertical scale in kilometers. Velocity increases downward everywhere in this section. Figure F9 shows a plot of the acoustic tomographic velocity with depth at Site 1096 (extracted from the section in Figure F8). The profile is compared with the nearest available stacking velocity (SP 1917, 650 m away from Site 1096) and with velocities obtained from core samples reduced to the same intervals as the tomographic velocities. At this site, there is a significant difference between the three profiles. The tomographic inversion produces values consistently ~200 m/s in excess of the PWS3 velocities, whereas the stacking velocity is higher than the laboratory measurements, as was observed at Site 1095. We think that the tomographic method here provides a better estimate of interval velocities than the stacking procedure. However, because of the limited offset compared to the depth of the objectives, tomography is sensitive to imperfections of the geometrical scheme used for inversion, thus introducing a systematic error. Therefore, we consider the PWS3 core profile to be the most reliable one for any application.

The data plotted in Figure F7 are provided in Table T3.

Site 1101

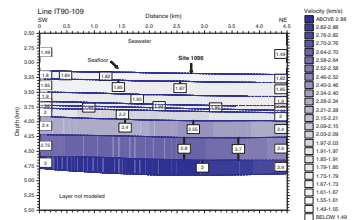
Only data from core measurements are available at Site 1101. Figure F10 displays the porosity, density, and velocity distributions with depth. Density and porosity display mirrored trends. Porosity decreases from ~70% at the seafloor to ~50% at 100 mbsf, showing a higher degree of compaction than at the other two sites. An increase of porosity downhole occurs below 100 mbsf, which brings the value to ~60% at the base of the hole (215 mbsf). The velocity distribution with depth is apparently not affected by the porosity and density distribution. Velocity increases steadily from ~1500 m/s at the seafloor to a little over 1600 m/s at the bottom of the hole.

All data plotted in Figure F10 are provided in Table T4.

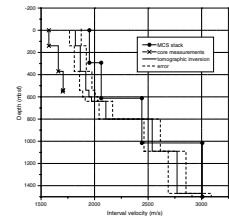
SEISMIC STRATIGRAPHY

At Site 1095, we tied MCS and borehole data using the velocities derived in situ with the velocity check shots and the vertical seismic profile. This is because this velocity estimation uses the same wavelength

F8. Tomographic inversion of traveltimes, Site 1096, p. 18.

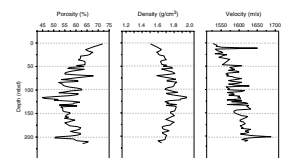


F9. Comparison among internal velocities, Site 1096, p. 19.



T3. Porosity, density, and velocity, Site 1096, p. 32.

F10. Comparison between IP porosity, IP density, and MST velocity, Site 1101, p. 20.



T4. Porosity, density, and velocity, Site 1101, p. 35.

and source as the one used in seismic reflection profiling (GI guns). This choice is strengthened by the good agreement between in situ velocity and velocity measured in the laboratory with high-frequency transducers. Figure F11 illustrates the velocity trend and its correlation to the seismic units described by Rebesco et al. (1997) and the lithostratigraphic units described on board (Shipboard Scientific Party, 1999b). The vertical seismic profile is tied to MCS seismics in Figure F12 according to position and strength of major reflectors. As shown in Figure F11, the uncertainty in correlation increases dramatically below the bottom of hole because of the extrapolation downward of the velocity trend. For the illustration in Figure F12, we chose the polynomial interpolation. Equations for both polynomial and linear interpolations are provided. A summary of the main tie points is illustrated in Figure F13. A list of tie points with values in two-way traveltime and depth units is additionally provided in Table T5.

The synthetic seismic trace obtained with the same methodology as described by the Shipboard Scientific Party (1999a) is compared with a compressed stacked section of seismic profile I95–135 around Site 1095 in Figure F14. The rather monotonous character of the seismic section in terms of frequencies and amplitudes prevents a firm statement about the quality of the match between synthetic and seismic traces.

At Site 1096, in the absence of in situ velocity measurements we produced a diagram similar to that shown in Figure F11 using the interval velocities obtained with the tomographic inversion of traveltimes. The resulting velocity trend and its correlation to the seismic units described by Rebesco et al. (1997) and the lithostratigraphic units described on board (Shipboard Scientific Party, 1999c) are presented in Figure F15. A list of tie points with values in two-way traveltime and meters below seafloor units is additionally provided in Table T5.

The synthetic seismic trace obtained with the same methodology as described by the Shipboard Scientific Party (1999a) is compared with a compressed stacked section of profile I95–135 around Site 1096 in Figure F16. The synthetic trace satisfactorily reproduces the alternation of packages of low- and high-amplitude reflectors as well as the decreasing frequency at the base of the hole.

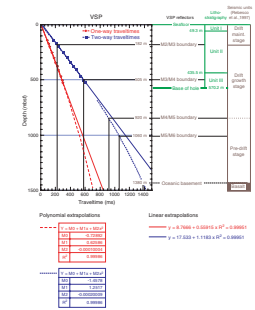
At Site 1101, the traveltime-depth relationship is derived from the laboratory PWS3 velocity data (Fig. F17). A list of tie points with values in two-way traveltime and depth units is additionally provided in Table T5.

CONCLUSIONS

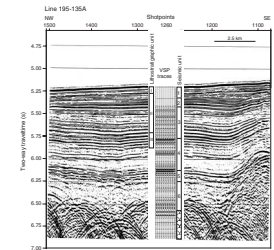
This report presents a revised composite set of density, porosity, and compressional velocity values derived from data obtained by various techniques.

Following comparative evaluation of overlapping data sets, we must conclude that in the continental rise sites drilled during ODP Leg 178, the downhole logging (performed only at Sites 1095 and 1096) did not provide reliable data, at least regarding sediment bulk density and porosity. This is in part because of poor hole conditions encountered in a fine-grained, generally underconsolidated formation and partly because of the bound water effect on neutron log porosity that was not completely removed. We suggest that logging while drilling could improve the quality of data if employed in this type of geological formation. Between core logging and laboratory measurements on core samples, we

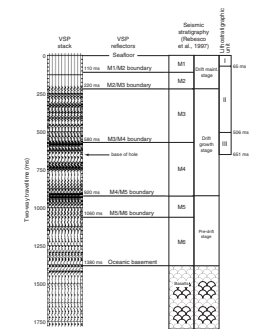
F11. Traveltimes and subbottom depth from the in situ velocity check shots, Site 1095, p. 21.



F12. Correlation between multi-channel and vertical seismic profile, Site 1095, p. 22.



F13. Vertical seismic profile and tie to two-way traveltimes, Site 1095, p. 23.



T5. Relationship between two-way traveltime and depth, p. 36.

prefer the latter. This is because the multiple-hole drilling strategy, and the generally good core recovery allowed the collection of a high number of evenly spaced measurements (generally one per core section) on cores. This offers the obvious advantage of the manual selection of samples and minimization of noise induced by core voids, biscuiting, and fracturing. Such noise is instead inevitably included in the automatic core-logging data sets, which, in spite of a much higher density of measurements (one every 4 cm), require complex noise removal.

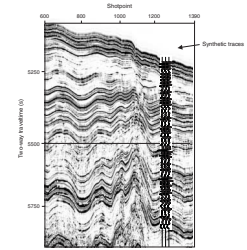
The vertical profiles of porosity and density allow us to identify anomalous consolidation trends at all three sites, probably induced by rapid sediment accumulation and/or the presence of biogenic silica in the sediment. Also, the velocity profiles obtained with vertical seismic profiles and tomographic inversion of traveltimes allowed us to perform a traveltime-depth correlation between site-survey MCS profiles and borehole data.

ACKNOWLEDGMENTS

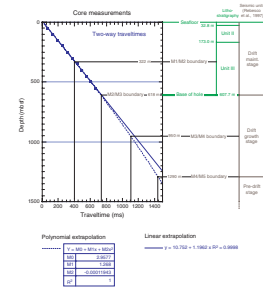
This work was made possible by cooperation among many persons, not all represented in the authorship. A. Vesnaver made the tomographic inversion codes available. F. Poletto allowed the performance of the VSP data processing. K.L. Hatfield and A.J. Evans (shipboard physical properties specialists) contributed with onboard data collection. L. Sormani and C. Pelos helped process OGS (Istituto Nazionale di Oceanografia e di Geofisica Sperimentale) site-survey MCS data. The manuscript was improved by the comments of Christian Bucker.

This study was funded by P.N.R.A (Progetto Nazionale di Ricerche in Antartide).

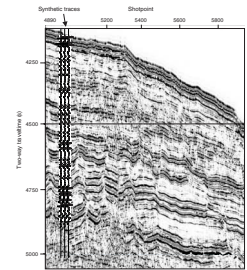
F14. Synthetic trace superimposed on Site 1095 MCS profile, p. 24.



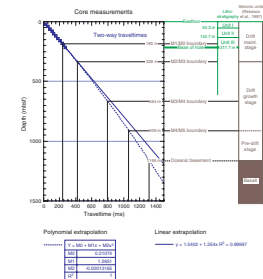
F15. Traveltimes and subbottom depth from core measurements, Site 1096, p. 25.



F16. Synthetic trace superimposed on Site 1096 MCS profile, p. 26.



F17. Traveltimes and subbottom depth from core measurements, Site 1101, p. 27.



REFERENCES

- Brogia, C., and Ellis, D., 1990. Effect of alteration, formation absorption, and stand-off on the response of the thermal neutron porosity log in gabbros and basalts: examples from Deep Sea Drilling Project-Ocean Drilling Program sites. *J. Geophys. Res.*, 95:9171–9188.
- Carrion, P., Vesnaver, A., Boehm, G., and Pettenati, F., 1993a. Aperture compensation tomography. *Geophys. Prospect.*, 41:367–380.
- Carrion, P., Boehm, G., Marchetti, A., Pettenati, F., and Vesnaver, A., 1993b. Reconstruction of lateral gradients from reflection tomography. *J. Seismic Expl.*, 5:55–67.
- Goldberg, D., 1997. The role of downhole measurements in marine geology and geophysics. *Rev. Geophys.*, 35:315–342.
- Hamilton, E.L., 1976. Variations of density and porosity with depth in deep-sea sediments. *J. Sediment. Petrol.*, 46:280–300.
- Rebesco, M., Larter, R.D., Barker, P.F., Camerlenghi, A., and Vanneste, L.E., 1997. The history of sedimentation on the continental rise west of the Antarctic Peninsula. In Barker, P.F., and Cooper, A.K. (Eds.), *Geology and Seismic Stratigraphy of the Antarctic Margin* (Pt. 2). Am. Geophys. Union, Antarctic Res. Ser., 71:29–50.
- Rebesco, M., Camerlenghi, A., and Zanolla, C., 1998. Bathymetry and morphogenesis of the continental margin west of the Antarctic Peninsula. *Terra Antart.*, 5:715–728.
- Shipboard Scientific Party, 1999a. Explanatory notes. In Barker, P.F., Camerlenghi, A., Acton, G.D., et al., *Proc. ODP, Init. Repts.*, 178, 1–66 [CD-ROM]. Available from: Ocean Drilling Program, Texas A&M University, College Station, TX 77845-9547, U.S.A.
- , 1999b. Site 1095. In Barker, P.F., Camerlenghi, A., Acton, G.D., et al., *Proc. ODP, Init. Repts.*, 178, 1–173 [CD-ROM]. Available from: Ocean Drilling Program, Texas A&M University, College Station, TX 77845-9547, U.S.A.
- , 1999c. Site 1096. In Barker, P.F., Camerlenghi, A., Acton, G.D., et al., *Proc. ODP, Init. Repts.*, 178, 1–144 [CD-ROM]. Available from: Ocean Drilling Program, Texas A&M University, College Station, TX 77845-9547, U.S.A.
- , 1999d. Site 1101. In Barker, P.F., Camerlenghi, A., Acton, G.D., et al., *Proc. ODP, Init. Repts.*, 178, 1–83 [CD-ROM]. Available from: Ocean Drilling Program, Texas A&M University, College Station, TX 77845-9547, U.S.A.
- Tinivella, U., Lodolo, E., Camerlenghi, A., and Boehm, G., 1998. Seismic tomography study of a bottom simulating reflector off the South Shetland Islands (Antarctica). In Henriot, J.-P., and Mienert, J. (Eds.), *Gas Hydrates: Relevance to World Margin Stability and Climate Change*. Sec. Publ.—Geol. Soc. London, 137:141–151.

Figure F1. Location map of ODP Sites 1095, 1096, and 1101 (shaded), together with all the other sites drilled during ODP Leg 178 (bathymetry after Rebesco et al., 1998). Short lines labeled a, b, and c indicate the approximate locations of MCS profiles as follows: a = Figures F4, p. 14, and F8, p. 18; b = Figures F12, p. 22, and F14, p. 24; c = Figure F16, p. 26. No seismic profiles are shown across Site 1101.

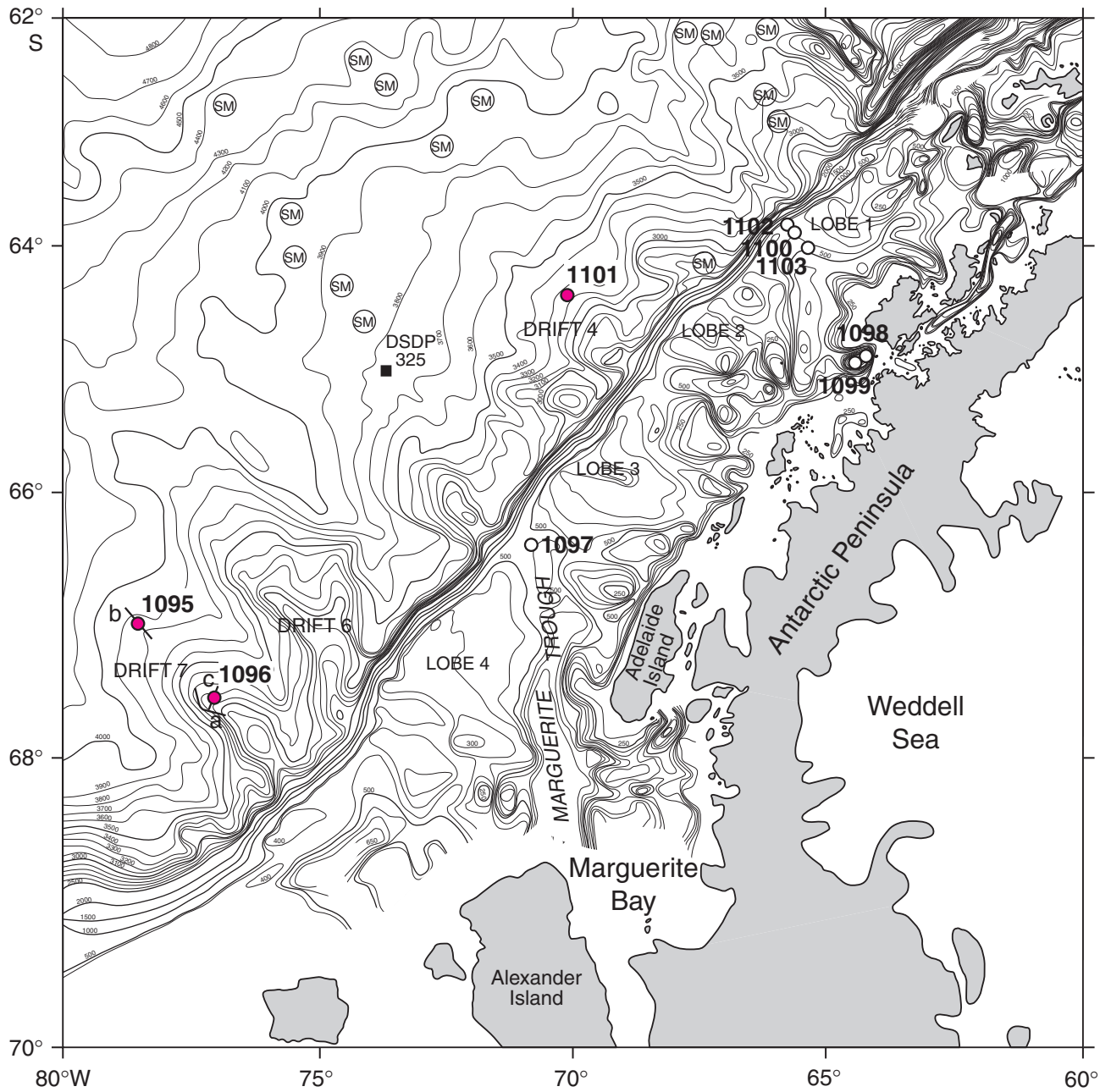


Figure F2. Example of raw data output from the MST core logger for sonic velocity. The large scatter is produced by voids, dropstones, and section edge effects. A substantial cleaning of data is necessary before use for seismic stratigraphic purposes (see “Core Logging and Core Sample Data,” p. 2, in “Methods”).

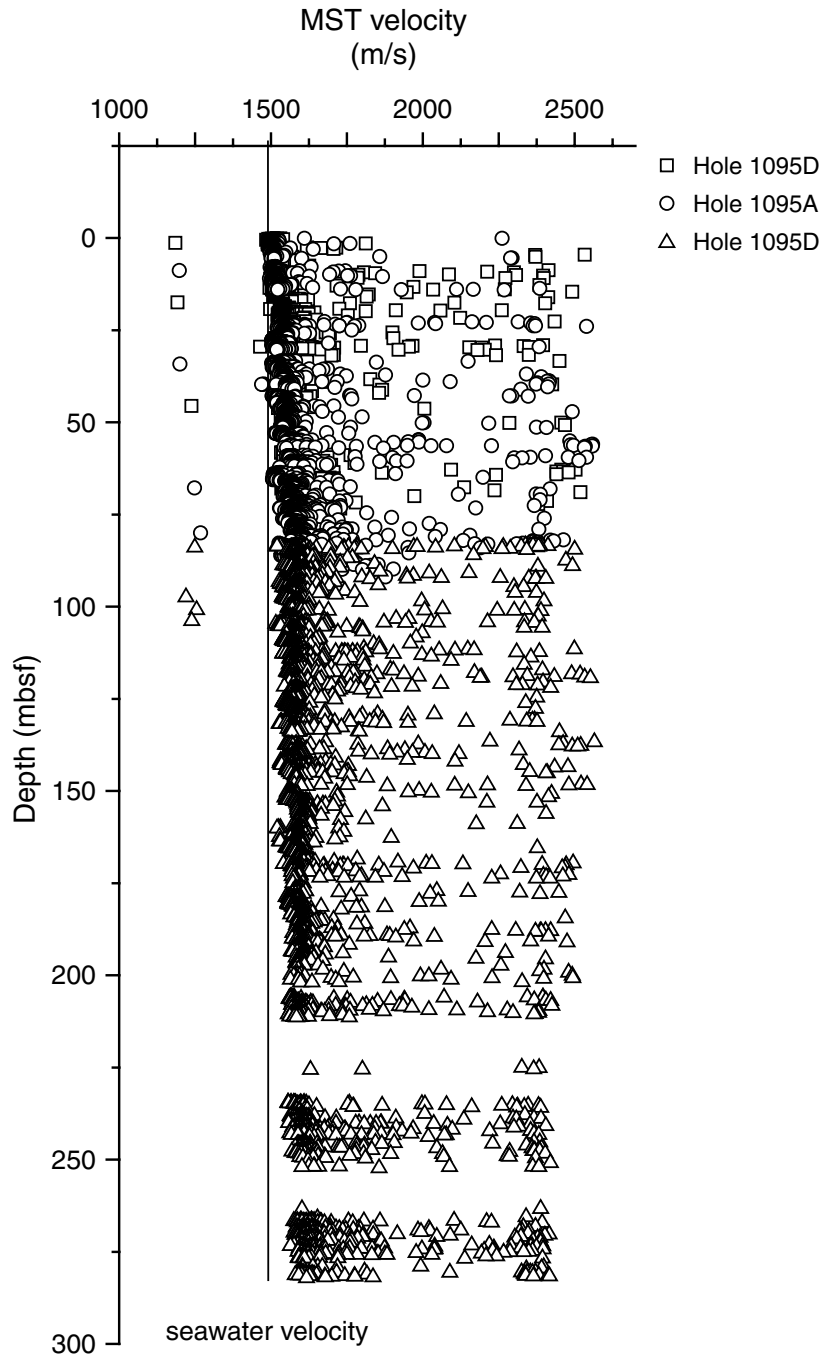


Figure F3. Example of error in PWS3 data files for Site 1095. The correction takes into account an erroneous parameter setting during acquisition. The file in Leg 178 *Initial Reports* volume contains the error (dashed line). The file in this report is corrected (solid line).

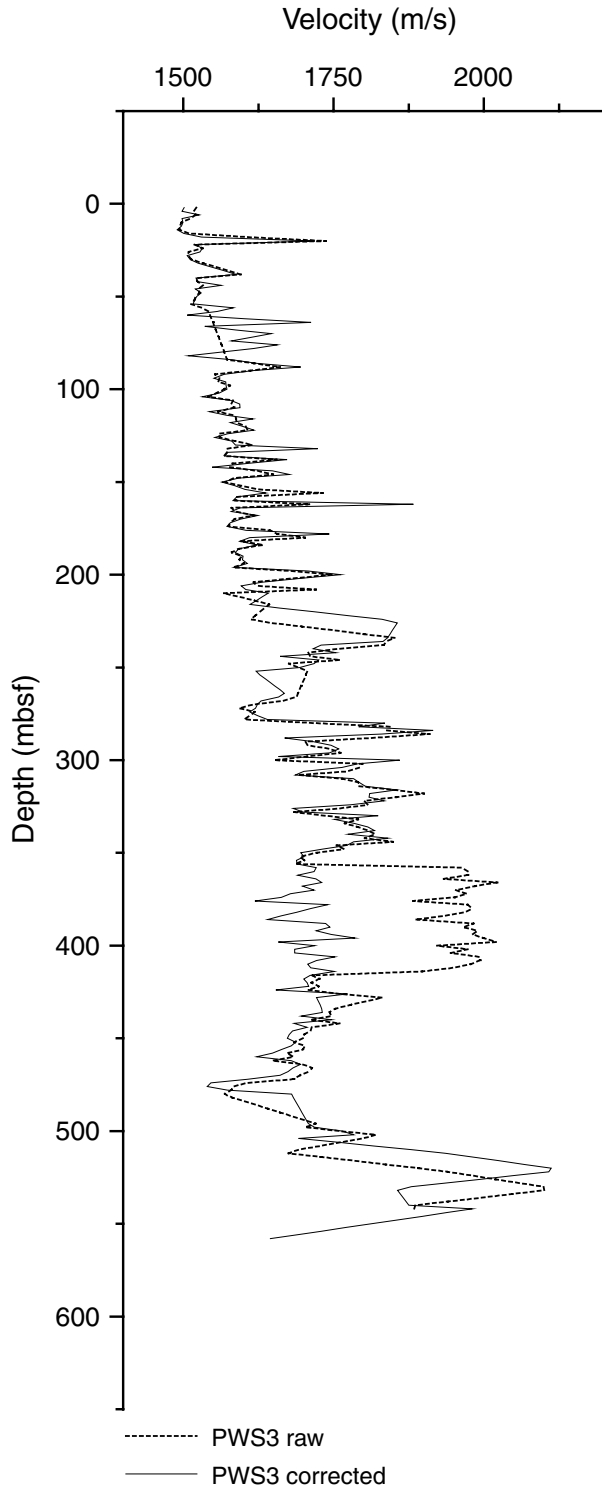


Figure F4. Picking of reflectors for the tomographic inversion of traveltimes at Site 1095. The diagram shows a display of shots as recorded by one trace 932.5 m from the source (see approximate location in Fig. F1, p. 11). Solid lines indicate the picked horizons. At the end of the inversion, each interval between picked horizons will be identified with a tomographic interval velocity (see Fig. F8, p. 18).

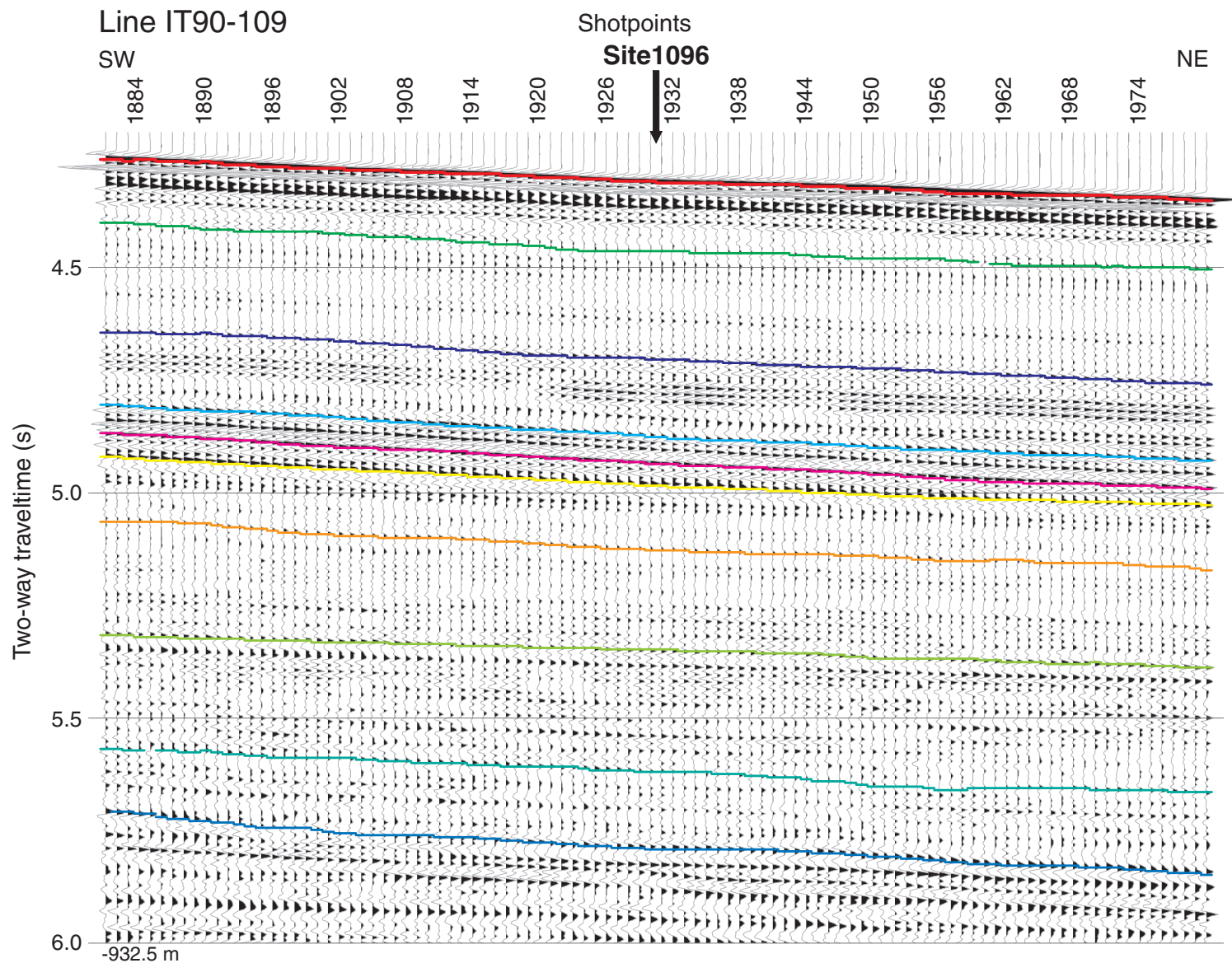


Figure F5. Comparison between downhole logging measurements (APLC porosity and RHOM density) and core logging measurements (index properties porosity and density and MST/PWS3 velocity) for Site 1095. There is no downhole velocity data.

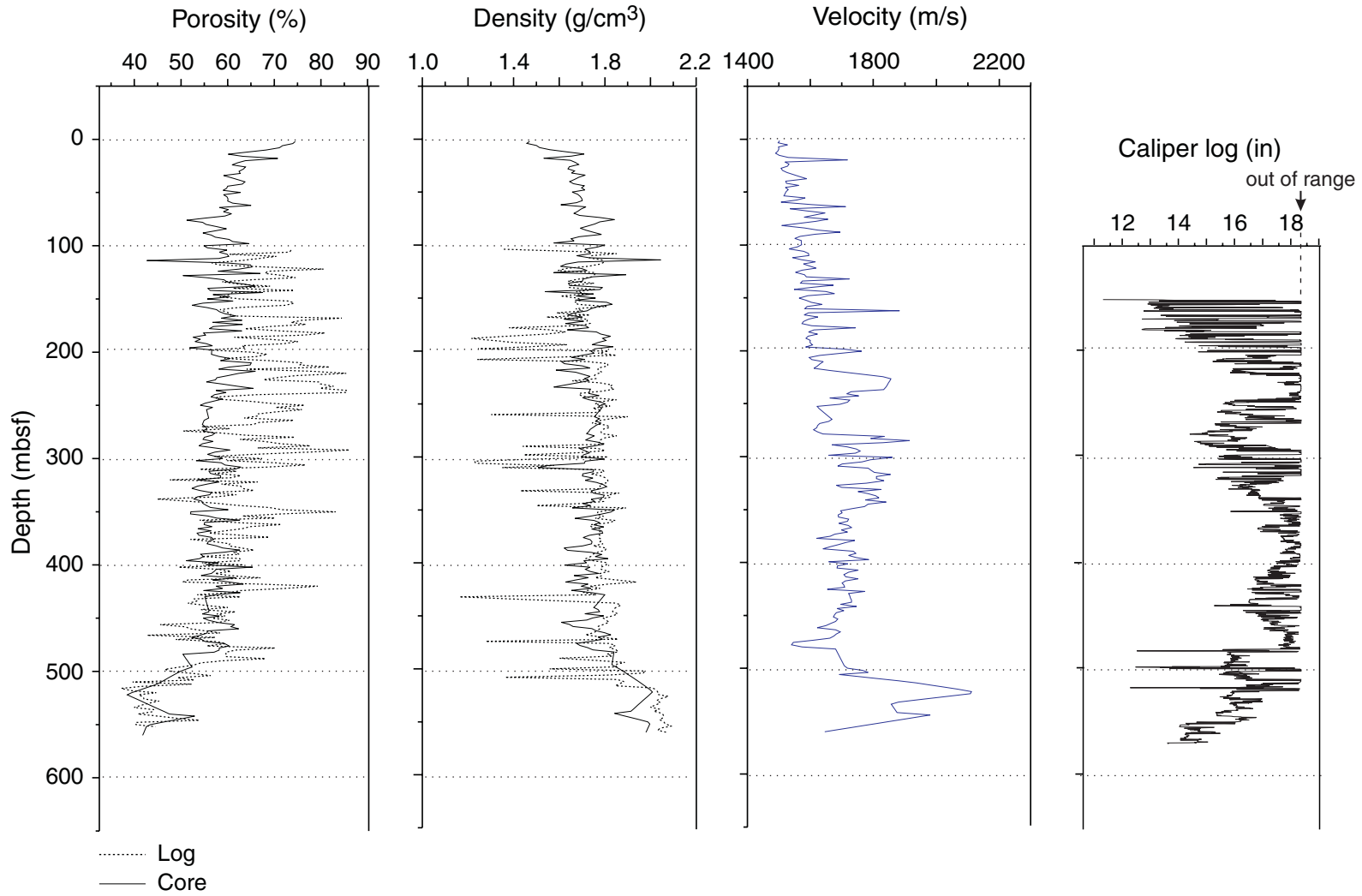


Figure F6. Comparison among interval velocities obtained with the in situ velocity check shots (during vertical seismic profiling), nearest available stacking velocities on MCS data, and velocity measured on cores (Fig. F5, p. 15) reduced to interval velocities with same intervals as velocity check shots for Site 1095 (see Table T1, p. 28). See “Results,” p. 5.

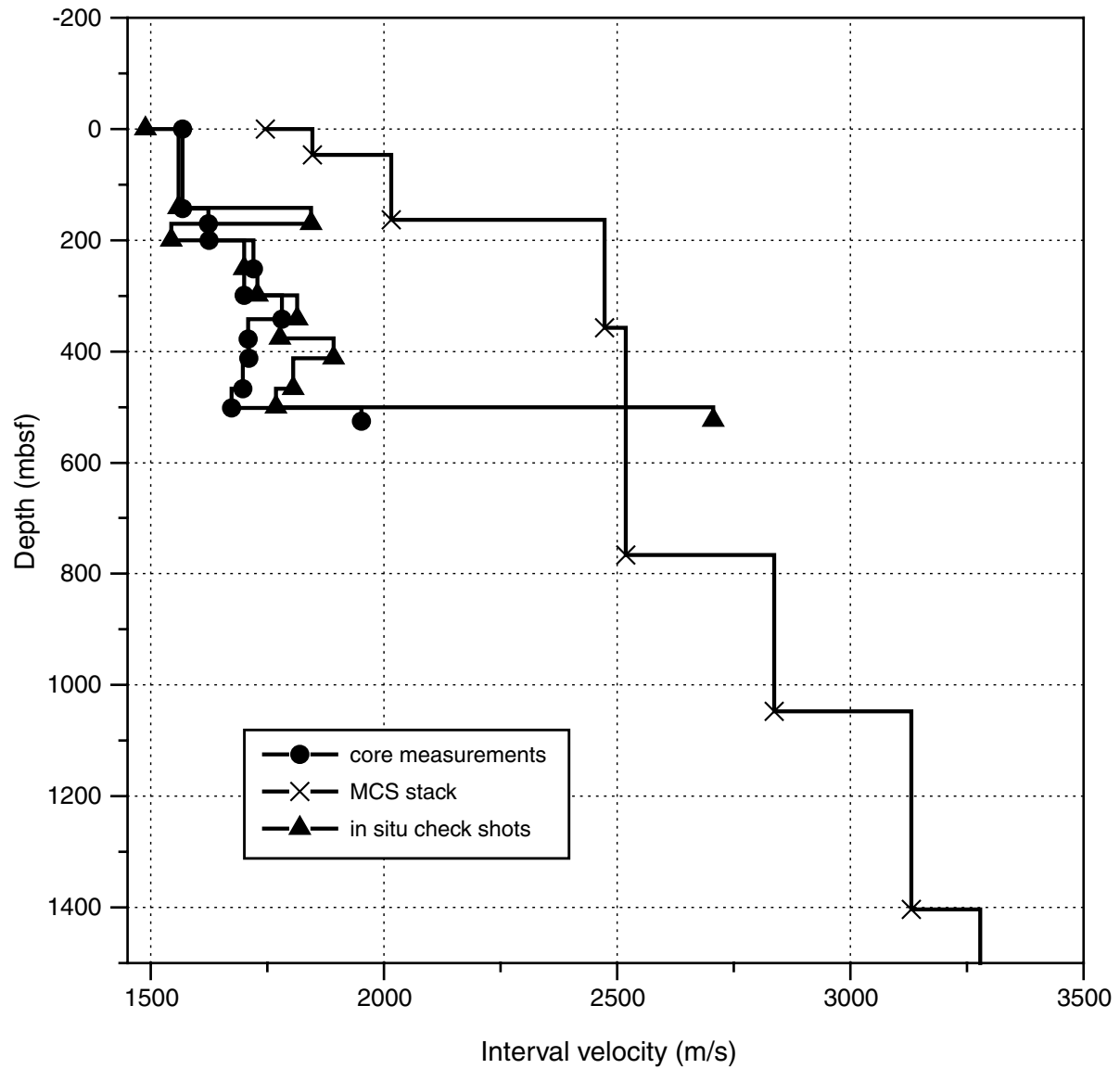


Figure F7. Comparison between downhole logging measurements (APLC porosity and RHOM density) and core logging measurements (index properties porosity and density and MST/PWS3 velocity) for Site 1096. There is no downhole velocity data.

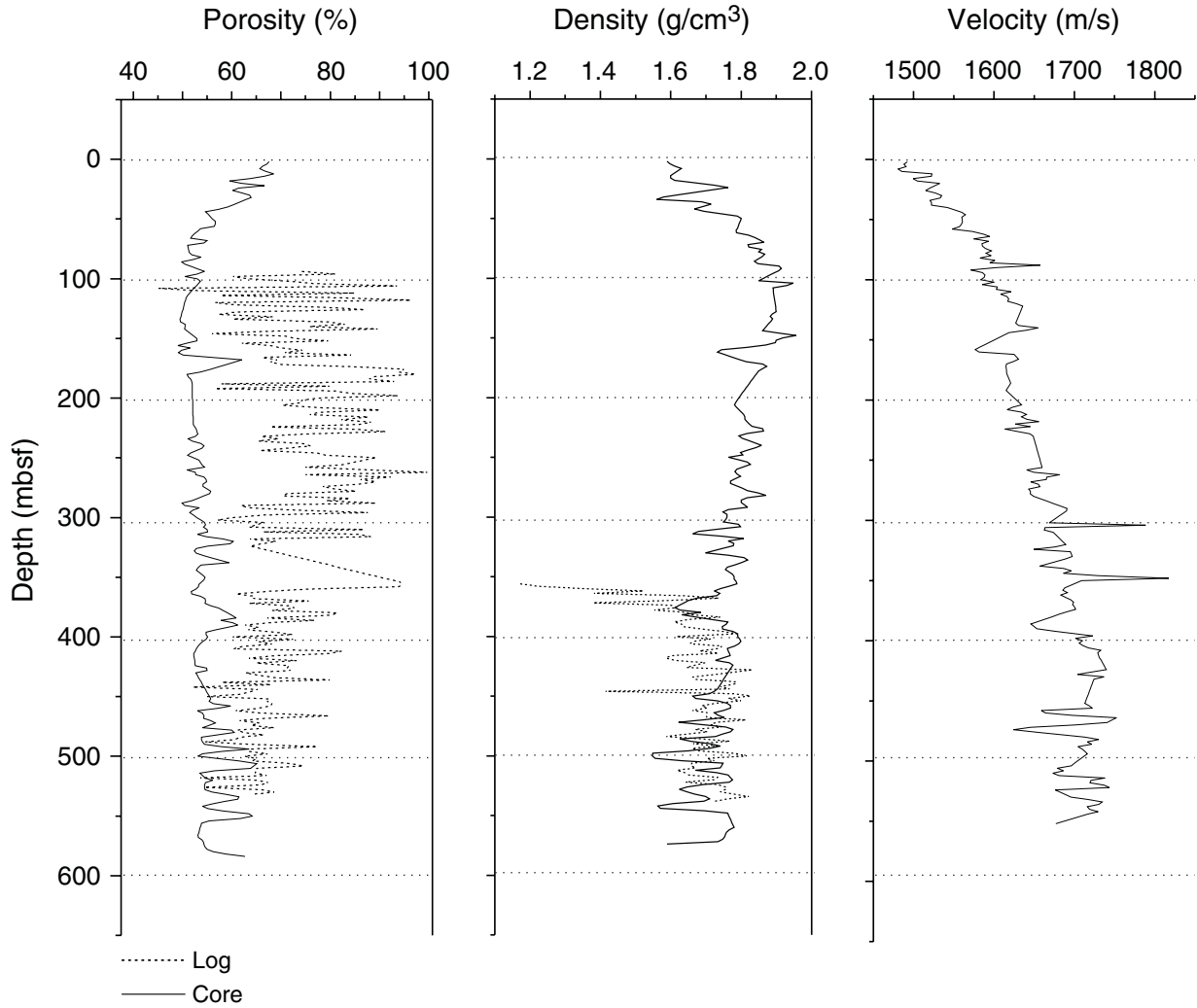


Figure F8. Results of tomographic inversion of traveltimes across Site 1096. The diagram shows the interval velocity, including lateral gradients, vs. depth. See the approximate location of the profile in Figure F1, p. 11.

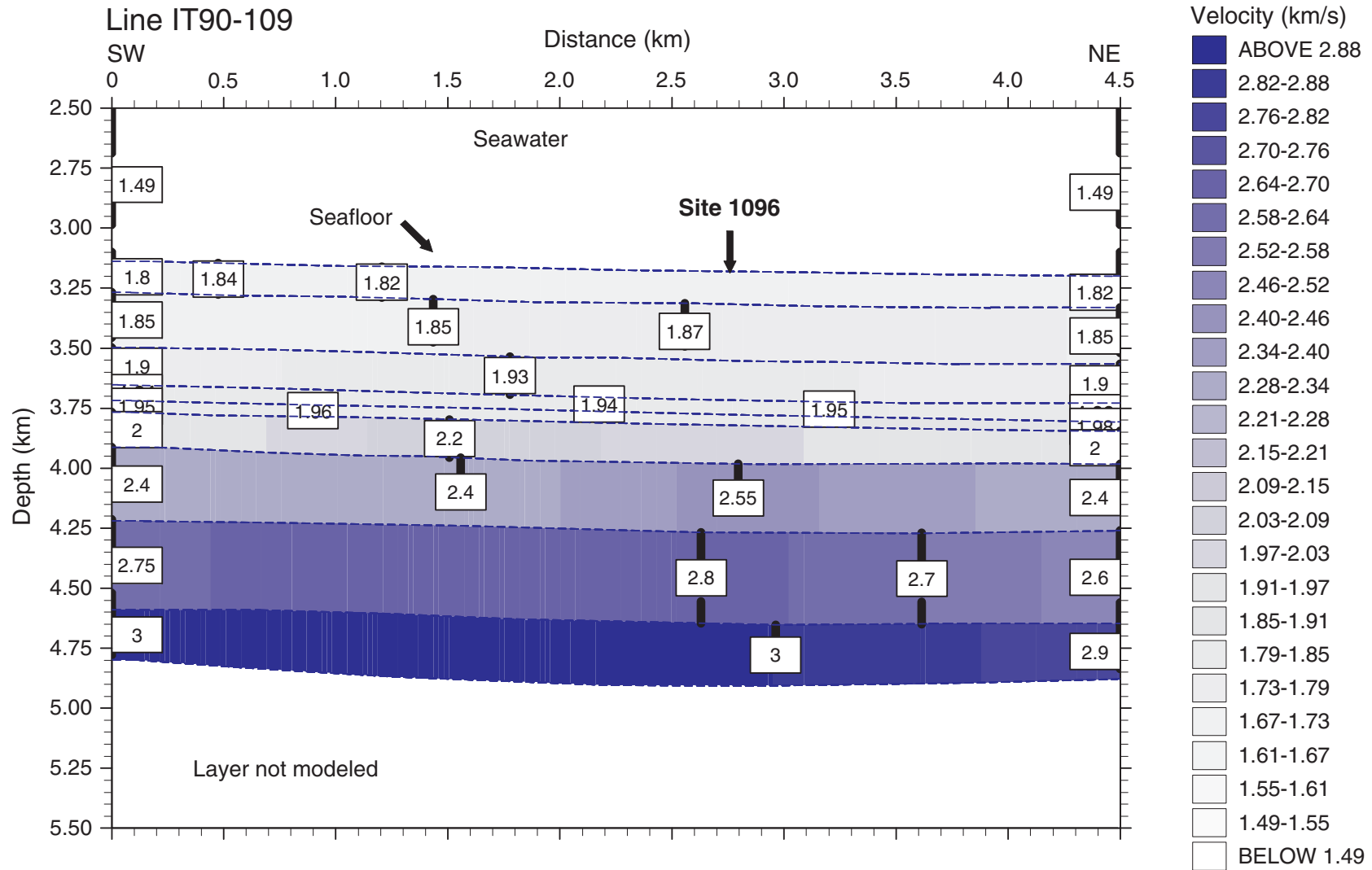


Figure F9. Comparison for Site 1096 among interval velocities obtained with the tomographic inversion (including error), nearest available stacking velocities on MCS data, and velocity measured on cores (Fig. F7, p. 17) reduced to interval velocities with same intervals as velocity check shots. See "Results," p. 5.

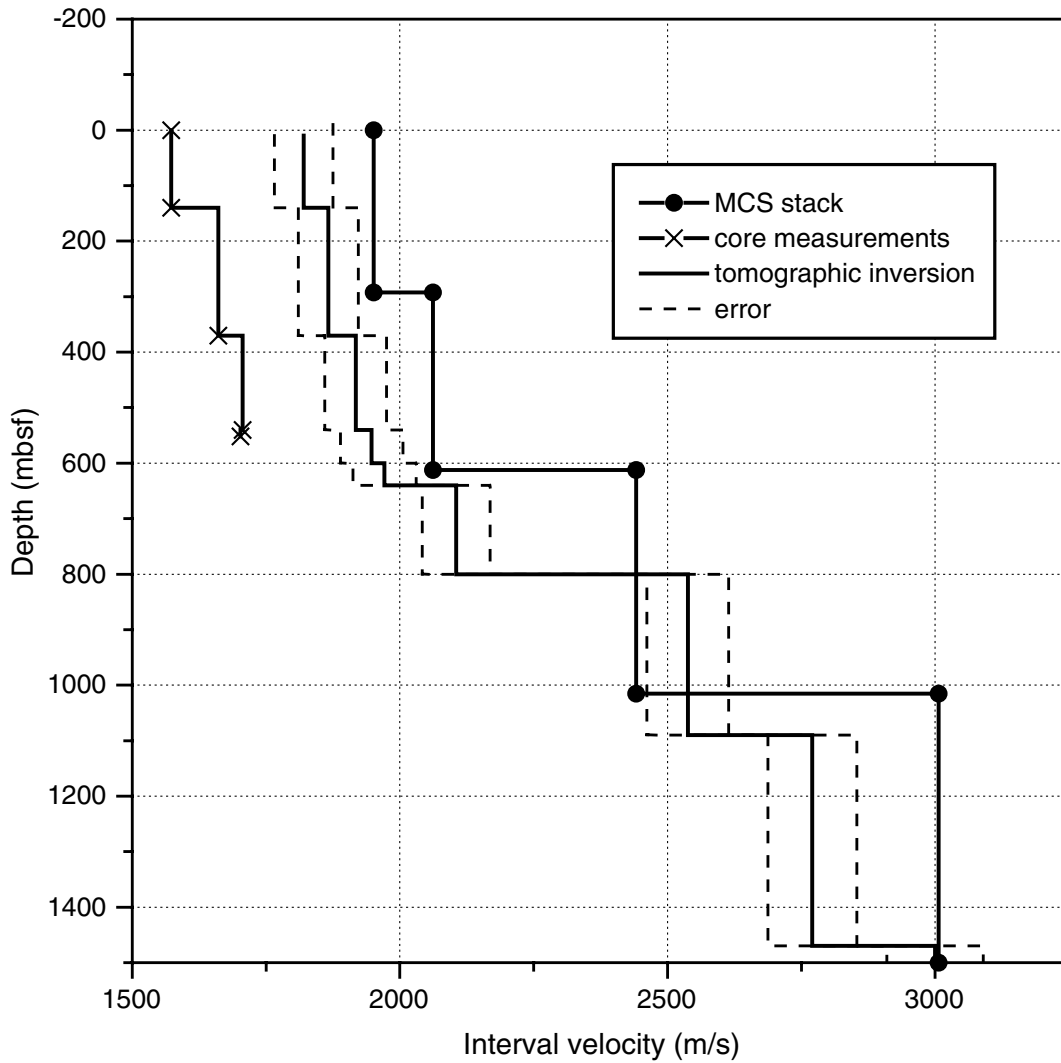


Figure F10. Comparison between index properties porosity and density and MST velocity for Site 1101. No downhole measurements are available for Site 1101.

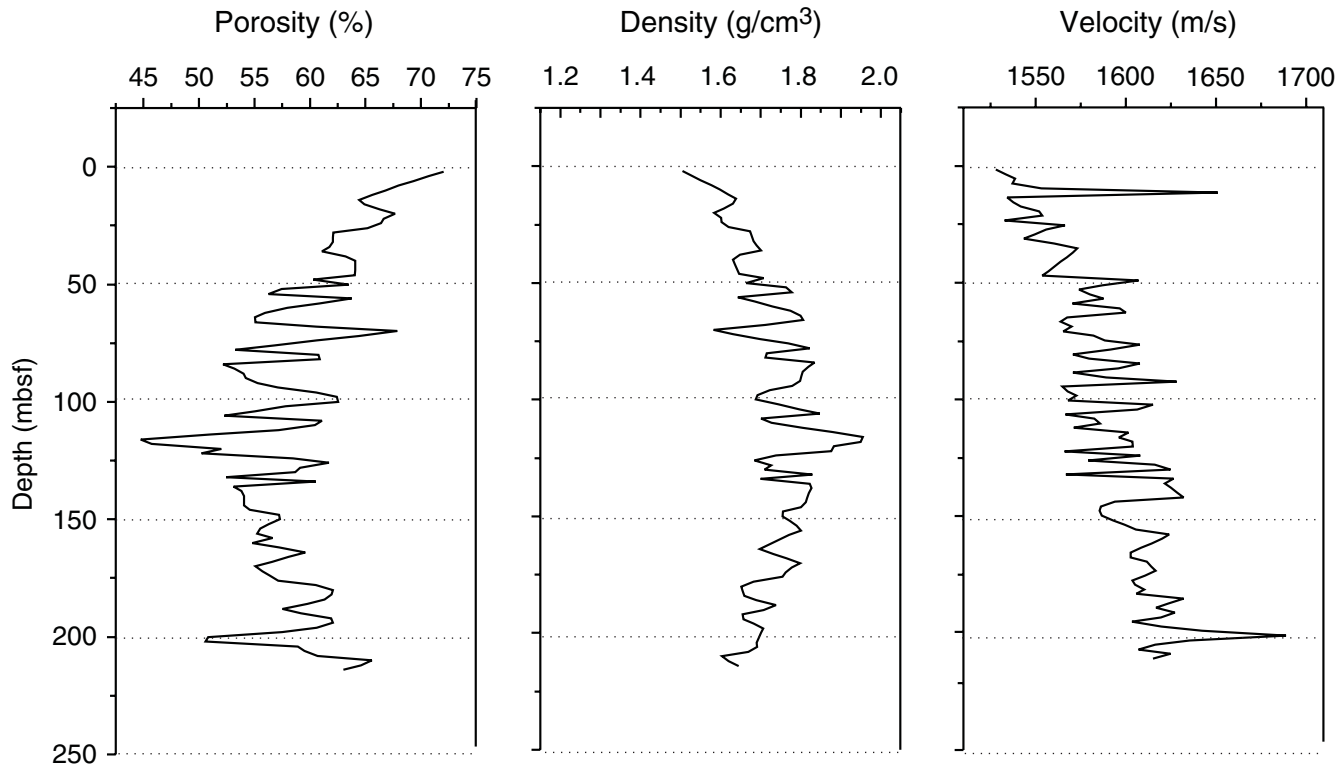
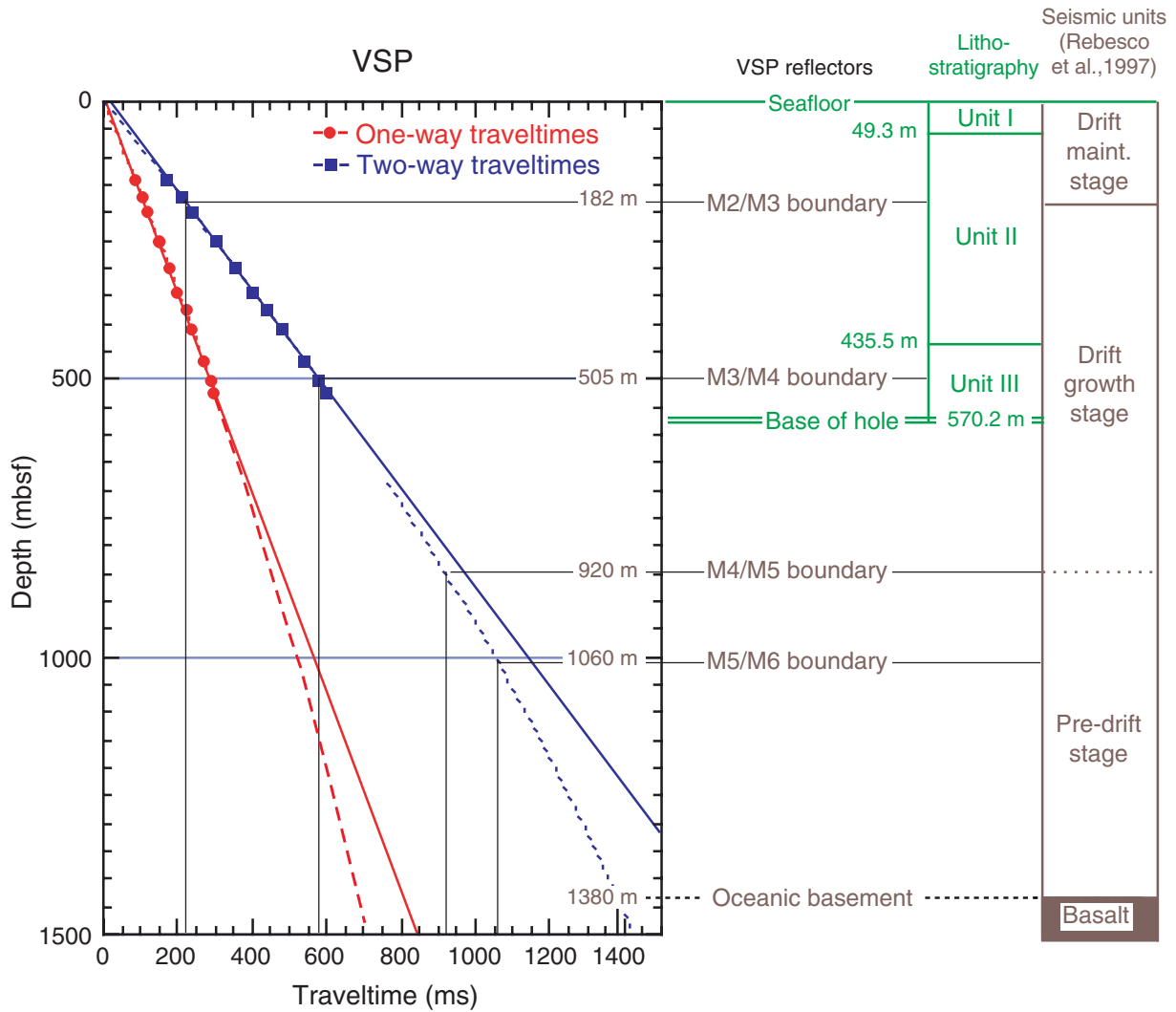


Figure F11. Plot of traveltimes and subbottom depth from the in situ velocity check shots for Site 1095. The equations of two velocity functions (linear and second-order polynomial) are provided. The diagram to the right summarizes the relationships in depth between lithostratigraphic and seismostratigraphic units.



Polynomial extrapolations

--- Y = M0 + M1x + M2x²

M0	-0.72892
M1	0.62586
M2	-0.00010004
R ²	0.99986

----- Y = M0 + M1x + M2x²

M0	-1.4578
M1	1.2517
M2	-0.00020009
R ²	0.99986

Linear extrapolations

— y = 8.7666 + 0.55915 x R² = 0.99951

— y = 17.533 + 1.1183 x R² = 0.99951

Figure F12. Correlation between onsite multichannel seismic and vertical seismic profiles for Site 1095. See the approximate location of the profile in Figure F1, p. 11.

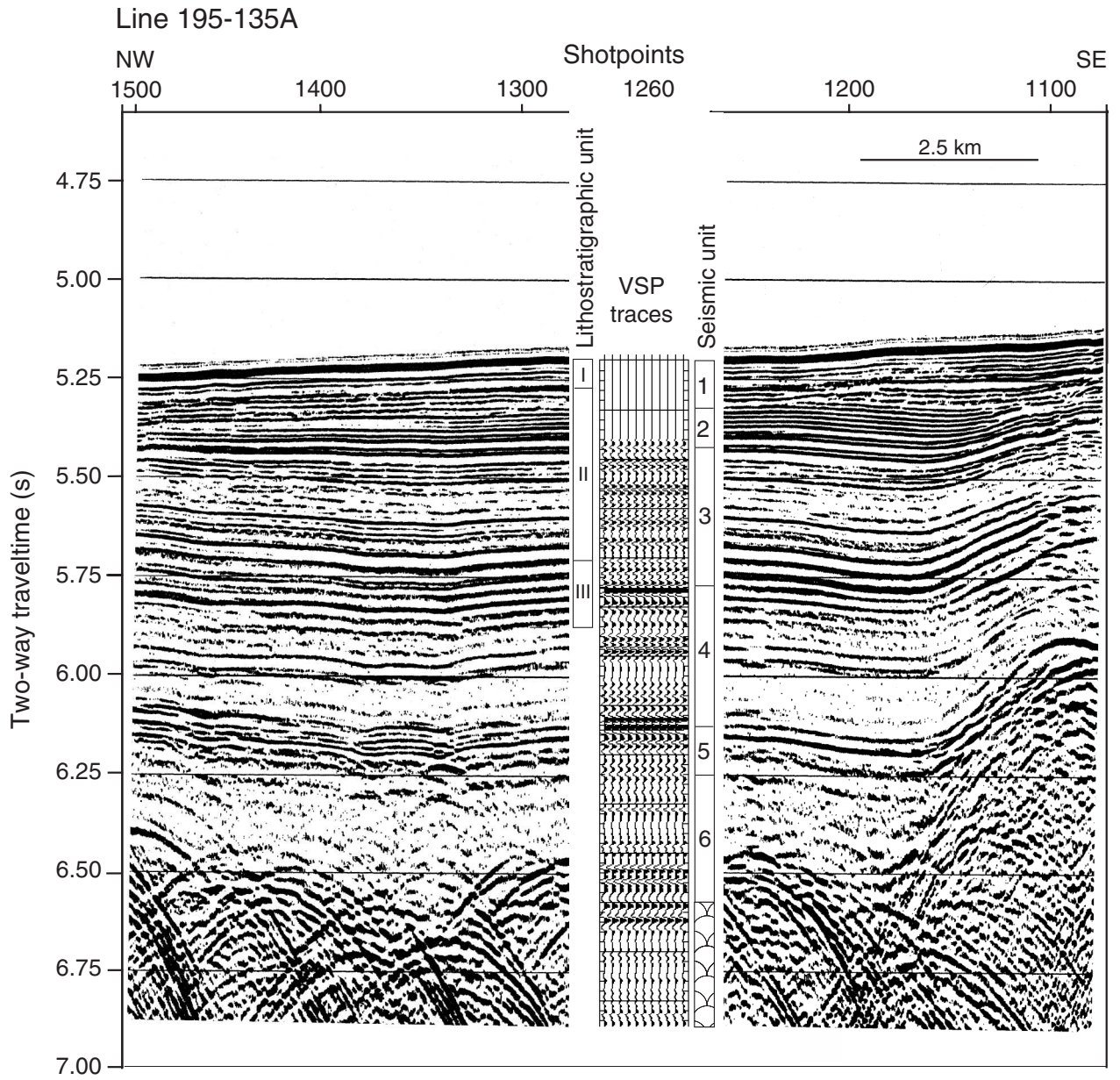


Figure F13. Vertical seismic profile and tie to two-way traveltimes between lithostratigraphic and seismostratigraphic units for Site 1095.

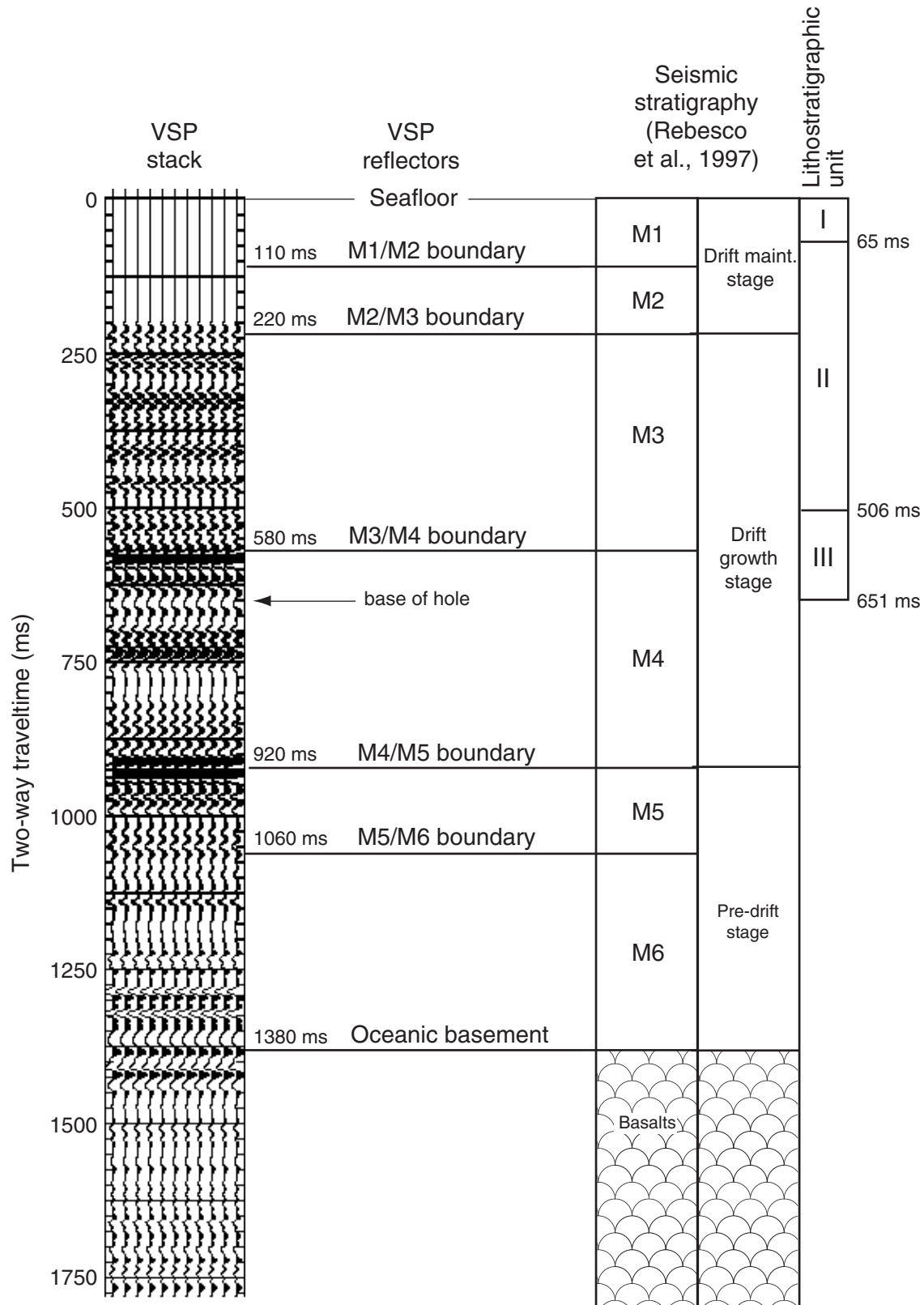


Figure F14. Synthetic trace superimposed on Site 1095 multichannel seismic profile. See the approximate location of the profile in Figure F1, p. 11.

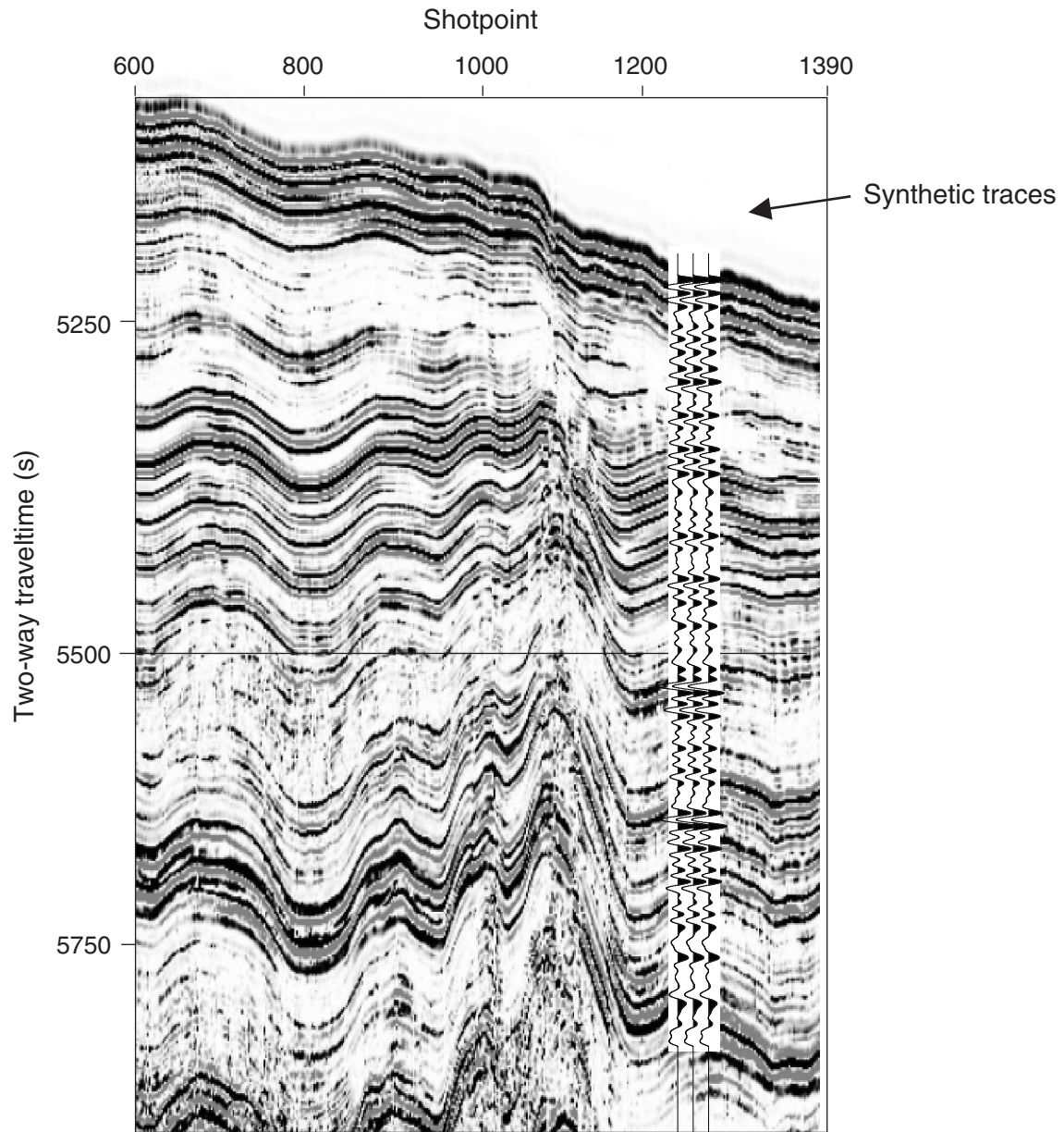
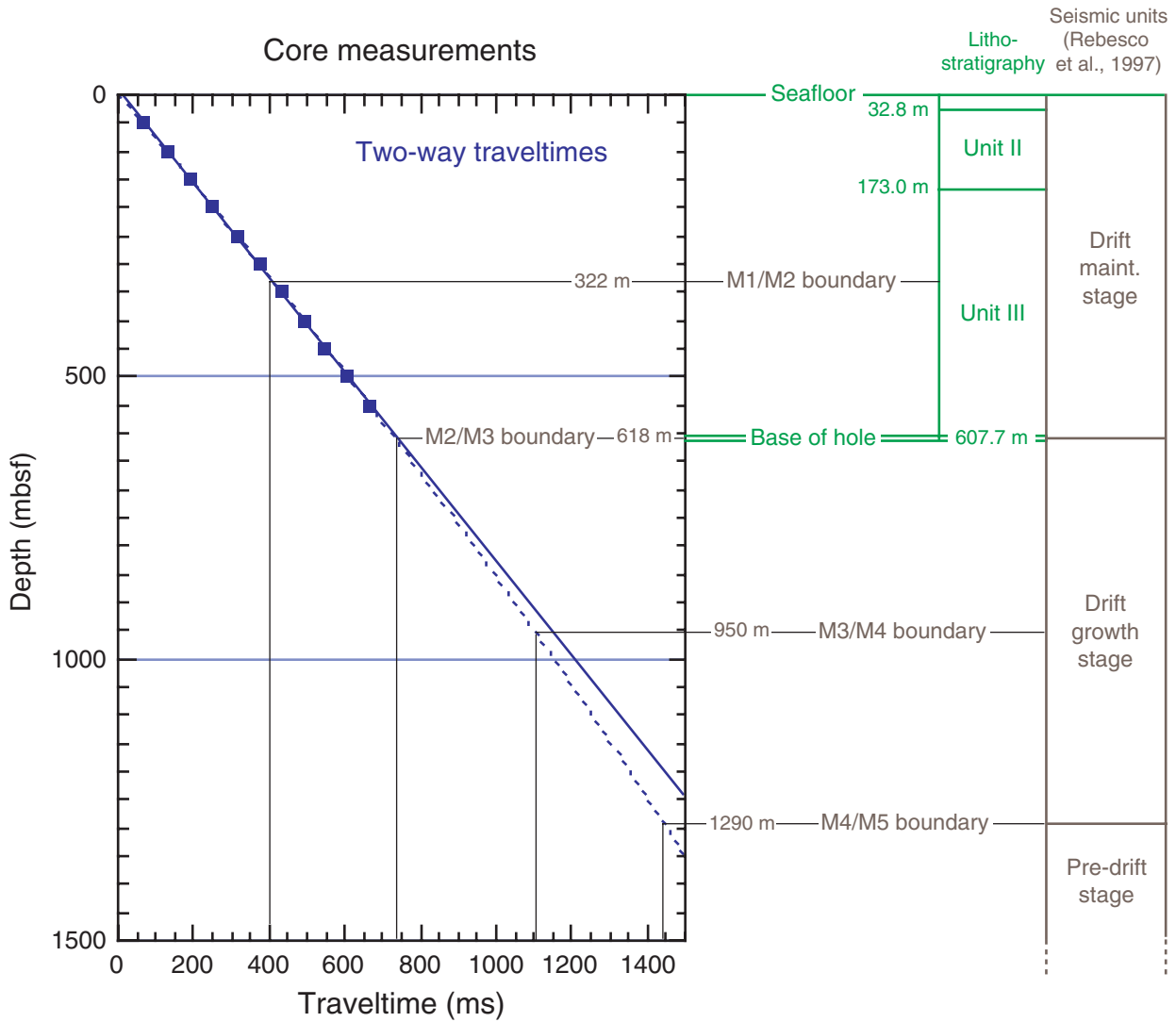


Figure F15. Plot of traveltimes and subbottom depth from core measurements (reduced to 50-m intervals) for Site 1096. The equations of two velocity functions (linear and second-order polynomial) are provided. The diagram to the right summarizes the relationships in depth between lithostratigraphic and seismostratigraphic units.



Polynomial extrapolation

$Y = M0 + M1x + M2x^2$	
M0	2.9577
M1	1.268
M2	-0.00011943
R ²	1

Linear extrapolation

————— $y = 10.752 + 1.1962 \times R^2 = 0.9998$

Figure F16. Synthetic trace superimposed on Site 1096 multichannel seismic profile. See the approximate location of the profile in Figure F1, p. 11.

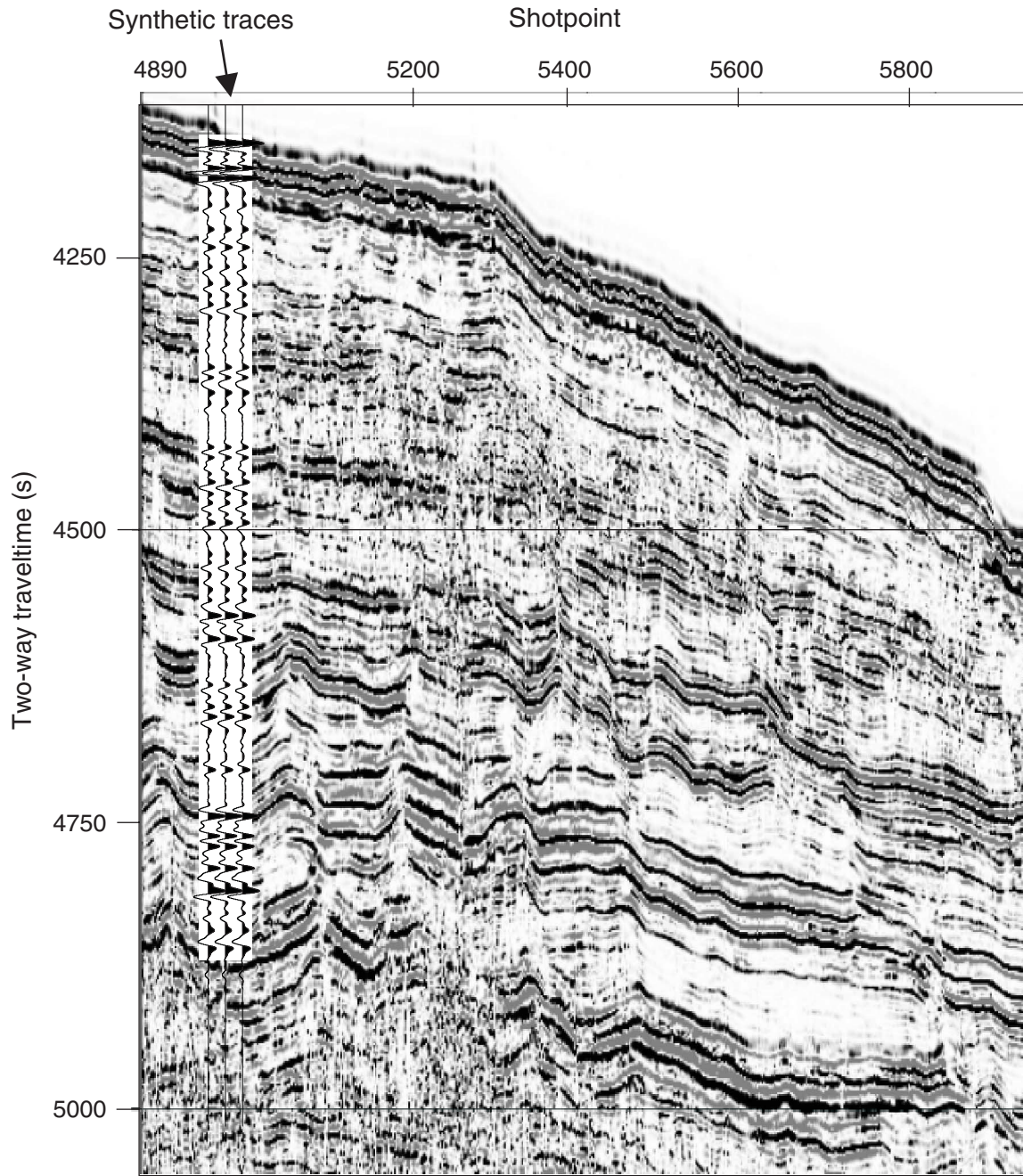
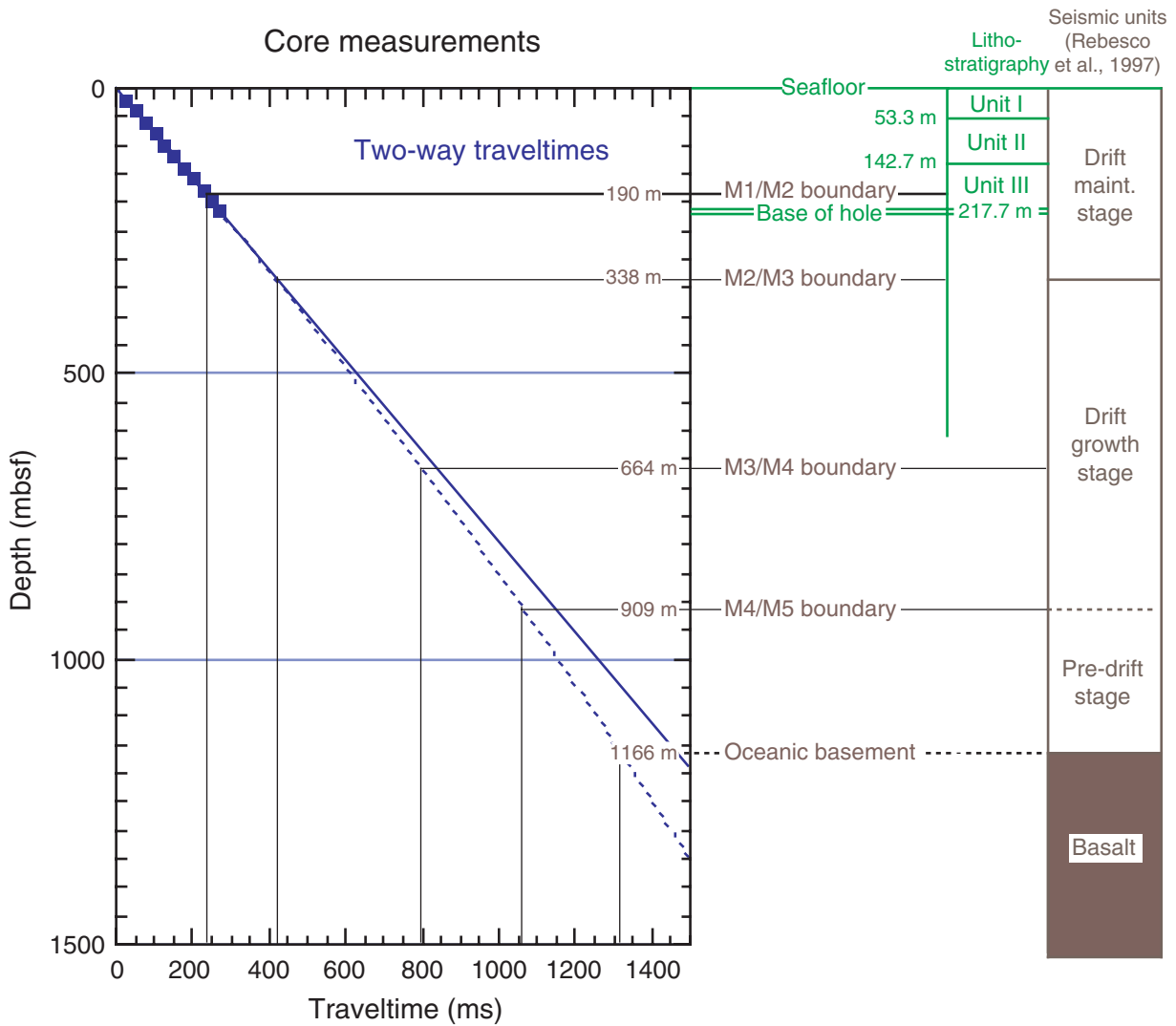


Figure F17. Plot of traveltimes and subbottom depth from core measurements (reduced to 20-m intervals) for Site 1101. The equations of two velocity functions (linear and second-order polynomial) are provided. The diagram to the right summarizes the relationships in depth between lithostratigraphic and seismostratigraphic units.



Polynomial extrapolation

$Y = M0 + M1x + M2x^2$	
M0	0.21074
M1	1.2851
M2	-0.00013165
R ²	1

Linear extrapolation

————— $y = 1.5402 + 1.254x$ R² = 0.99997

Table T1. Parts of data sets used to compile the composite profiles from core data.

Core	Interval (mbsf)	Measurement
Velocity:		
1095D	2.22-82.52	PWS3
1095B	83.47-281.55	MST
1095B	209.86-561.23	PWS3
Density and porosity:		
1095A	0.05-78.86	IP
1095B	83.43-561.34	IP
Velocity:		
1096B	0.11-37.40	PWS2
1096B	45.50-256.64	PWS3
1096C	117.48-553.56	PWS3
Density and porosity:		
1096A	1.36-138.26	IP
1096B	109.21-255.74	IP
1096C	114.58-583.60	IP
Velocity:		
1101A	1.23-215.70	PWS3
Density and porosity:		
1101A	0.15-215.39	IP

Note: IP = index properties, MST = multisensor track, PWS2 and PWS3 = Hamilton frame velocity probes.

Table T2. Core and downhole logs of porosity, density, and velocity, Site 1095. (Continued on next two pages.)

Depth (mbsf)	Core log			Downhole log		Depth (mbsf)	Core log			Downhole log	
	Porosity (%)	Density (g/cm ³)	Velocity (m/s)	Porosity (%)	Density (g/cm ³)		Porosity (%)	Density (g/cm ³)	Velocity (m/s)	Porosity (%)	Density (g/cm ³)
2	74.5	1.4	1501.7			136	63.6	1.64	1569.2	62.4	1.75
4	73.9	1.45	1497.8			138	66.0	1.65	1672.7	69.1	1.65
6	71.7	1.5	1526.8			140	55.7	1.79	1605.0	61.2	1.64
8	71.0	1.51	1498.2			142	56.3	1.78	1548.1	74.2	1.76
10	68.2	1.55	1499.6			144	67.6	1.54	1648.7	61.0	1.67
12	64.0	1.63	1496.8			146	56.9	1.75	1676.8	60.6	1.72
14	60.1	1.7	1490.0			148	60.5	1.67	1591.8	58.3	1.61
16	63.2	1.65	1501.1			150	55.6	1.76	1564.2	62.9	1.68
18	70.7	1.53	1530.1			152	61.2	1.67	1585.7	73.1	1.70
20	63.7	1.64	1718.5			154	54.7	1.81	1602.7	74.2	1.67
22	62.1	1.67	1519.8			156	52.4	1.83	1637.5	72.5	1.68
24	60.9	1.68	1531.6			158	55.5	1.77	1588.9	62.3	1.81
26	63.8	1.64	1527.6			160	57.6	1.74	1582.8	58.4	1.67
28	63.3	1.63	1506.5			162	58.3	1.72	1883.0	59.5	1.70
30	62.4	1.66	1511.4			164	59.5	1.67	1594.3	60.7	1.59
32	62.7	1.65	1524.7			166	61.8	1.64	1580.0	60.6	1.73
34	59.1	1.71	1545.7			168	58.6	1.70	1624.1	84.5	1.54
36	60.7	1.68	1566.7			170	63.1	1.62	1595.6	75.9	1.72
38	62.2	1.66	1587.7			172	56.8	1.71	1578.3	73.6	1.72
40	63.6	1.64	1521.3			174	63.2	1.63	1572.8	76.8	1.74
42	63.1	1.66	1524.1			176	56.9	1.71	1604.4	68.9	1.69
44	59.9	1.7	1563.3			178	56.1	1.73	1743.1	63.7	1.38
46	59.7	1.69	1520.3			180	63.0	1.64	1610.7	71.3	1.56
48	59.0	1.71	1530.0			182	54.8	1.76	1593.9	80.9	1.63
50	62.7	1.65	1522.2			184	55.2	1.78	1622.9	76.4	1.55
52	59.0	1.68	1519.1			186	52.6	1.82	1592.4	61.4	1.37
54	59.8	1.69	1516.2			188	54.2	1.79	1586.3	69.1	1.21
56	60.0	1.69	1583.2			190	53.0	1.80	1599.5	75.1	1.31
58	60.0	1.7	1556.3			192	55.5	1.77	1598.7	72.1	1.41
60	61.0	1.67	1506.3			194	56.8	1.74	1606.8	63.1	1.63
62	65.0	1.6	1602.7			196	51.8	1.84	1584.3	63.9	1.47
64	58.2	1.71	1712.6			198	56.6	1.76	1708.0	55.9	1.24
66	60.1	1.69	1535.8			200	56.6	1.74	1762.2	65.3	1.82
68	59.1	1.68	1587.1			202	56.5	1.75	1696.2	68.5	1.77
70	60.8	1.66	1646.2			204	58.1	1.70	1630.2	66.4	1.85
72	59.3	1.68	1613.4			206	60.6	1.65	1596.4	59.3	1.56
74	55.1	1.77	1580.4			208	58.5	1.71	1603.8	68.9	1.24
76	51.2	1.84	1656.3			210	65.1	1.61	1641.4	76.1	1.72
78	54.6	1.77	1616.9			212	64.8	1.62	1631.2	75.5	1.81
80	55.3	1.75	1562.7			214	60.4	1.70	1621.1	81.8	1.81
82	57.5	1.72	1508.5			216	58.1	1.73	1611.0	64.1	1.77
84	59.7	1.69	1580.8			218	66.0	1.59	1660.2	78.0	1.77
86	57.2	1.71	1622.8			220	62.4	1.67	1717.1	85.5	1.79
88	54.6	1.75	1695.3			222	60.0	1.70	1774.1	74.7	1.76
90	56.4	1.78	1614.5			224	57.7	1.74	1831.0	70.4	1.75
92	57.3	1.68	1568.0			226	57.4	1.71	1855.9	67.7	1.76
94	60.3	1.65	1550.9			228	55.4	1.73	1851.9	79.7	1.66
96	61.0	1.66	1570.5			230	58.8	1.68	1847.9	79.9	1.78
98	64.5	1.57	1571.1			232	62.1	1.63	1843.9	82.7	1.83
100	54.9	1.8	1572.5			234	65.5	1.58	1839.9	79.8	1.82
102	55.6	1.76	1559.5			236	57.5	1.74	1832.4	85.7	1.84
104	59.8	1.71	1531.7	73.6	1.36	238	59.7	1.73	1729.1	85.3	1.79
106	58.2	1.73	1579.2	73.2	1.68	240	57.2	1.73	1716.1	66.3	1.69
108	59.9	1.73	1594.0	60.4	1.85	242	56.4	1.77	1753.9	57.8	1.69
110	60.2	1.68	1594.6	70.5	1.74	244	58.9	1.70	1661.3	57.4	1.74
112	58.1	1.73	1543.3	66.7	1.73	246	57.1	1.73	1725.4	64.5	1.85
114	42.7	2.04	1572.2	62.9	1.79	248	55.2	1.78	1717.7	68.9	1.78
116	59.6	1.68	1616.2	56.6	1.80	250	54.1	1.80	1693.3	76.5	1.76
118	64.9	1.63	1578.1	58.1	1.78	252	56.8	1.77	1621.3	70.3	1.82
120	65.2	1.61	1598.0	68.4	1.72	254	55.5	1.79	1627.2	75.9	1.75
122	62.5	1.70	1617.6	80.5	1.63	256	55.6	1.78	1635.6	70.7	1.78
124	58.0	1.72	1573.6	68.6	1.59	258	55.7	1.77	1644.0	66.5	1.76
126	67.0	1.58	1552.6	68.0	1.76	260	55.8	1.76	1652.5	66.5	1.30
128	50.4	1.89	1581.0	72.0	1.75	262	55.9	1.75	1660.9	63.5	1.90
130	55.4	1.75	1586.7	74.5	1.74	264	55.0	1.78	1668.4	74.2	1.82
132	59.2	1.70	1723.6	65.1	1.69	266	54.8	1.76	1658.5	66.7	1.77
134	59.8	1.70	1574.3	58.8	1.64	268	54.6	1.78	1629.1	65.4	1.74

Table T2 (continued).

Depth (mbsf)	Core log			Downhole log		Depth (mbsf)	Core log			Downhole log	
	Porosity (%)	Density (g/cm ³)	Velocity (m/s)	Porosity (%)	Density (g/cm ³)		Porosity (%)	Density (g/cm ³)	Velocity (m/s)	Porosity (%)	Density (g/cm ³)
270	55.2	1.76	1623.0	54.4	1.81	406	57.1	1.71	1752.5	60.7	1.78
272	55.5	1.75	1620.1	60.4	1.82	408	56.5	1.73	1721.6	57.3	1.82
274	54.7	1.74	1610.5	50.5	1.79	410	54.3	1.77	1707.1	60.3	1.78
276	57.3	1.73	1623.2	58.8	1.78	412	61.8	1.67	1712.0	67.1	1.79
278	56.7	1.72	1639.8	63.8	1.79	414	56.8	1.73	1751.6	51.5	1.76
280	55.0	1.75	1835.2	74.4	1.85	416	60.3	1.67	1711.2	50.4	1.85
282	54.7	1.73	1791.8	62.6	1.80	418	63.4	1.63	1700.4	66.8	1.94
284	56.9	1.72	1915.4	67.8	1.78	420	57.5	1.73	1706.2	79.3	1.82
286	54.6	1.77	1830.5	71.3	1.77	422	58.9	1.70	1708.5	72.1	1.73
288	53.8	1.80	1668.9	77.7	1.80	424	54.8	1.74	1653.9	62.8	1.78
290	57.2	1.74	1716.3	66.4	1.44	426	62.7	1.65	1773.5	60.5	1.72
292	60.5	1.69	1745.7	86.1	1.77	428	57.5	1.74	1721.7	53.5	1.71
294	57.3	1.71	1758.5	77.5	1.80	430	55.1	1.80	1724.6	62.7	1.76
296	55.7	1.73	1743.3	65.4	1.68	432	55.2	1.79	1727.6	52.7	1.16
298	57.5	1.71	1658.5	57.2	1.45	434	55.4	1.78	1730.5	53.4	1.39
300	59.0	1.70	1860.2	67.4	1.81	436	55.5	1.78	1731.1	51.5	1.62
302	53.2	1.80	1790.3	59.9	1.50	438	55.6	1.77	1696.5	55.3	1.85
304	58.6	1.71	1763.9	70.1	1.23	440	55.8	1.76	1746.3	60.1	1.87
306	59.4	1.71	1700.5	76.7	1.23	442	56.0	1.75	1684.4	54.3	1.85
308	62.9	1.55	1686.5	68.3	1.58	444	56.0	1.77	1706.1	61.7	1.84
310	61.6	1.51	1783.3	54.0	1.35	446	54.6	1.78	1681.9	57.7	1.83
312	56.0	1.75	1792.6	61.9	1.79	448	58.2	1.71	1676.3	59.5	1.86
314	56.3	1.75	1802.8	57.2	1.80	450	54.8	1.79	1673.2	56.7	1.84
316	58.5	1.70	1854.9	62.8	1.74	452	55.9	1.75	1686.8	60.4	1.79
318	58.5	1.70	1810.0	60.6	1.78	454	57.9	1.72	1680.0	58.0	1.80
320	53.5	1.75	1809.3	47.6	1.80	456	61.5	1.61	1663.7	45.5	1.82
322	58.2	1.71	1834.2	66.5	1.81	458	60.7	1.64	1648.7	50.9	1.79
324	55.7	1.76	1778.1	58.6	1.81	460	62.4	1.66	1622.1	52.0	1.77
326	53.5	1.79	1682.7	62.9	1.78	462	55.7	1.74	1679.7	55.2	1.78
328	52.3	1.81	1699.6	63.2	1.78	464	55.6	1.76	1695.1	58.4	1.76
330	54.1	1.78	1824.2	65.6	1.78	466	54.1	1.80	1682.3	42.7	1.75
332	56.5	1.74	1751.6	56.1	1.43	468	52.3	1.83	1674.5	57.4	1.71
334	56.2	1.75	1783.7	61.9	1.86	470	54.4	1.77	1661.3	48.9	1.79
336	53.5	1.80	1807.2	57.7	1.81	472	55.2	1.79	1607.6	57.7	1.86
338	52.8	1.79	1818.1	44.9	1.82	474	59.4	1.74	1545.8	59.6	1.28
340	54.5	1.74	1774.3	51.3	1.77	476	60.3	1.68	1539.7	55.5	1.82
342	54.7	1.76	1840.4	57.6	1.79	478	58.2	1.69	1573.7	70.2	1.85
344	55.4	1.70	1783.4	62.0	1.69	480	58.2	1.72	1680.1	61.7	1.82
346	56.3	1.74	1771.5	68.8	1.50	482	57.1	1.75	1683.6	59.6	1.85
348	60.1	1.66	1732.0	71.7	1.89	484	50.4	1.84	1687.1	59.7	1.86
350	52.1	1.84	1695.7	83.2	1.82	486	50.7	1.84	1690.5	59.6	1.81
352	52.0	1.83	1700.9	71.5	1.77	488	51.1	1.84	1694.0	68.1	1.83
354	55.8	1.78	1688.3	63.2	1.77	490	51.4	1.84	1697.5	59.0	1.60
356	57.7	1.73	1689.6	70.1	1.79	492	51.7	1.83	1701.0	54.3	1.75
358	62.6	1.67	1721.4	54.0	1.76	494	52.0	1.83	1704.5	52.8	1.89
360	55.1	1.75	1717.8	61.4	1.85	496	52.4	1.83	1708.0	49.9	1.84
362	55.0	1.78	1690.6	71.5	1.82	498	51.0	1.85	1718.3	46.5	1.85
364	56.6	1.75	1720.6	64.8	1.73	500	49.8	1.86	1765.2	47.9	1.56
366	53.6	1.79	1730.2	63.1	1.74	502	49.0	1.88	1783.3	52.7	1.97
368	56.4	1.74	1698.3	59.4	1.78	504	48.2	1.89	1692.0	56.4	1.97
370	53.5	1.79	1717.6	56.0	1.78	506	47.3	1.91	1754.5	49.2	1.81
372	53.9	1.79	1678.3	62.8	1.77	508	46.5	1.92	1817.1	52.9	1.36
374	56.5	1.73	1663.0	68.9	1.78	510	45.7	1.93	1879.6	39.6	1.86
376	57.0	1.70	1619.1	52.0	1.77	512	44.9	1.95	1936.1	52.3	1.88
378	55.9	1.73	1740.7	56.9	1.79	514	43.6	1.96	1980.1	42.1	1.86
380	55.6	1.74	1711.8	60.5	1.78	516	42.2	1.97	2024.0	37.2	1.85
382	57.6	1.74	1689.1	60.3	1.79	518	40.8	1.99	2067.9	39.3	2.01
384	58.9	1.70	1662.8	62.9	1.75	520	39.4	2.00	2111.9	44.7	2.02
386	62.6	1.62	1640.3	65.6	1.81	522	38.5	2.01	2107.9	40.9	2.03
388	59.4	1.64	1736.6	61.2	1.80	524	39.5	2.00	2050.8	41.9	2.03
390	54.2	1.74	1744.0	62.5	1.77	526	40.5	1.99	1993.6	42.0	2.08
392	54.8	1.79	1721.2	54.5	1.75	528	41.5	1.98	1936.5	45.3	2.05
394	54.0	1.76	1745.9	62.6	1.74	530	42.5	1.97	1879.3	43.0	2.03
396	51.2	1.81	1786.0	62.8	1.72	532	43.5	1.96	1856.5	41.3	2.04
398	58.0	1.71	1657.9	54.5	1.75	534	44.5	1.95	1861.2	39.9	2.03
400	55.4	1.72	1718.9	63.3	1.81	536	45.5	1.94	1865.9	44.3	2.00
402	65.4	1.62	1685.6	49.5	1.80	538	46.5	1.92	1870.7	43.8	2.04
404	57.6	1.73	1685.1	57.9	1.78	540	47.5	1.91	1875.4	40.8	2.01

Table T2 (continued).

Depth (mbsf)	Core log			Downhole log	
	Porosity (%)	Density (g/cm ³)	Velocity (m/s)	Porosity (%)	Density (g/cm ³)
542	52.9	1.84	1980.6	45.1	2.05
544	50.7	1.88	1938.7	49.0	2.06
546	48.3	1.91	1896.8	53.9	2.06
548	45.9	1.95	1854.8	40.3	2.04
550	43.4	1.99	1812.9	40.3	2.06
552	42.6	2.00	1771.0	44.6	2.06
554	42.4	1.99	1729.1		2.09
556	42.2	1.99	1687.1		2.04
558	42.0	1.98	1645.2		2.03
560	41.8	1.98			2.07

Table T3. Core and downhole logs of porosity, density, and velocity, Site 1096. (Continued on next two pages.)

Depth (mbsf)	Core log			Downhole log		Depth (mbsf)	Core log			Downhole log	
	Porosity (%)	Density (g/cm ³)	Velocity (m/s)	Porosity (%)	Density (g/cm ³)		Porosity (%)	Density (g/cm ³)	Velocity (m/s)	Porosity (%)	Density (g/cm ³)
2	67.6	1.59	1492.1			136	49.6	1.88	1629.8	79.5	
4	67.1	1.60	1488.3			138	50.5	1.88	1628.9	83.0	
6	66.2	1.61	1496.7			140	50.5	1.87	1628.1	75.8	
8	65.7	1.63	1480.8			142	50.4	1.87	1627.2	89.7	
10	66.7	1.62	1488.9			144	51.0	1.86	1626.3	66.7	
12	68.5	1.61	1522.8			146	51.6	1.91	1625.4	55.9	
14	66.6	1.60	1522.4			148	52.3	1.96	1624.5	71.0	
16	63.7	1.60	1500.1			150	52.9	1.92	1623.6	72.7	
18	59.5	1.61	1500.7			152	52.9	1.90	1622.7	79.6	
20	62.0	1.67	1531.7			154	50.8	1.90	1621.9	62.0	
22	66.6	1.72	1505.5			156	49.0	1.87	1621.0	67.9	
24	61.5	1.76	1504.5			158	51.5	1.82	1620.1	70.1	
26	60.2	1.72	1515.1			160	49.8	1.74	1619.2	74.4	
28	61.9	1.67	1527.1			162	49.1	1.73	1618.3	70.7	
30	63.7	1.62	1535.0			164	50.1	1.75	1617.4	84.3	
32	63.9	1.58	1533.1			166	56.0	1.77	1616.5	66.2	
34	62.7	1.56	1520.5			168	62.1	1.79	1615.7	69.2	
36	61.5	1.69	1522.2			170	60.5	1.81	1614.8	67.8	
38	60.4	1.71	1521.4			172	58.9	1.86	1615.7	70.2	
40	59.2	1.69	1540.5			174	57.3	1.87	1616.9	85.5	
42	57.2	1.67	1549.3			176	55.7	1.86	1618.1	95.0	
44	54.7	1.69	1558.1			178	53.6	1.85	1619.3	94.0	
46	55.2	1.74	1566.9			180	50.9	1.84	1620.5	97.3	
48	55.6	1.79	1560.0			182	51.2	1.84	1621.6	88.6	
50	56.0	1.80	1560.6			184	51.7	1.83	1622.8	88.0	
52	56.6	1.80	1560.9			186	51.9	1.83	1624.0	93.1	
54	56.7	1.80	1559.5			188	51.9	1.82	1625.2	57.9	
56	56.5	1.79	1556.9			190	51.9	1.82	1626.4	79.9	
58	53.6	1.79	1548.1			192	52.0	1.81	1627.6	56.6	
60	53.1	1.79	1573.2			194	52.0	1.81	1628.8	81.0	
62	52.5	1.79	1586.6			196	52.0	1.80	1629.9	84.1	
64	52.0	1.82	1594.8			198	52.0	1.80	1631.1	93.8	
66	51.7	1.84	1581.1			200	52.0	1.79	1632.3	77.2	
68	54.9	1.85	1593.2			202	52.0	1.79	1633.5	74.1	
70	54.4	1.86	1585.0			204	52.0	1.78	1634.7	74.1	
72	51.0	1.82	1585.7			206	52.1	1.78	1623.0	70.2	
74	51.1	1.82	1589.2			208	52.1	1.79	1616.4	77.3	
76	51.2	1.86	1596.8			210	52.1	1.79	1633.6	90.1	
78	51.3	1.85	1586.6			212	52.1	1.80	1640.4	77.9	
80	51.9	1.87	1584.0			214	52.1	1.81	1634.3	75.8	
82	53.7	1.86	1585.8			216	52.1	1.81	1640.6	87.8	
84	52.2	1.85	1601.2			218	52.2	1.81	1655.7	82.1	
86	49.7	1.84	1594.8			220	52.2	1.82	1626.5	88.4	
88	50.5	1.85	1657.6			222	52.2	1.82	1645.2	85.6	
90	51.8	1.91	1603.1			224	52.5	1.83	1613.7	67.9	
92	53.1	1.91	1571.2			226	52.8	1.86	1628.9	85.3	
94	54.4	1.91	1585.5	74.2		228	52.9	1.86	1644.1	91.3	
96	52.9	1.89	1588.9	81.1		230	53.1	1.82	1648.8	75.1	
98	50.5	1.88	1587.9	60.2		232	52.6	1.79	1649.7	66.0	
100	53.0	1.86	1583.7	63.6		234	51.1	1.80	1650.5	69.5	
102	53.6	1.85	1600.1	71.7		236	52.0	1.82	1651.4	65.4	
104	53.2	1.95	1585.3	76.6		238	53.8	1.84	1652.2	74.4	
106	52.7	1.93	1604.1	93.6		240	54.4	1.86	1653.1	76.0	
108	52.3	1.89	1602.9	45.1		242	54.0	1.84	1653.9	71.2	
110	51.9	1.89	1621.4	53.3		244	52.8	1.82	1654.8	65.7	
112	51.4	1.89	1608.2	84.9		246	51.7	1.80	1655.6	77.3	
114	51.0	1.89	1616.1	57.8		248	51.1	1.81	1656.5	79.2	
116	50.7	1.89	1618.4	82.4		250	52.2	1.76	1657.3	89.5	
118	50.6	1.90	1617.1	96.4		252	53.3	1.79	1658.1	112.5	
120	50.5	1.90	1628.1	56.7		254	53.6	1.82	1659.0	107.9	
122	50.3	1.90	1636.0	60.9		256	54.0	1.83	1659.8	82.3	
124	50.2	1.90	1635.1	79.1		258	54.5	1.81	1640.6	74.9	
126	50.0	1.90	1634.3	87.0		260	50.9	1.79	1649.6	88.2	
128	49.9	1.90	1633.4	60.8		262	52.6	1.78	1681.4	99.8	
130	49.8	1.89	1632.5	57.2		264	52.7	1.79	1665.9	75.0	
132	49.6	1.88	1631.6	68.3		266	54.3	1.80	1669.0	92.3	
134	49.5	1.89	1630.7	60.2		268	54.8	1.78	1645.7	86.0	

Table T3 (continued).

Depth (mbsf)	Core log			Downhole log		Depth (mbsf)	Core log			Downhole log	
	Porosity (%)	Density (g/cm ³)	Velocity (m/s)	Porosity (%)	Density (g/cm ³)		Porosity (%)	Density (g/cm ³)	Velocity (m/s)	Porosity (%)	Density (g/cm ³)
270	54.9	1.77	1655.4	89.2		406	53.5	1.79	1717.5	68.2	1.65
272	54.2	1.77	1657.0	85.8		408	53.1	1.78	1733.1	62.3	1.75
274	54.1	1.79	1643.2	78.4		410	52.8	1.76	1729.0	60.4	1.74
276	55.0	1.80	1645.4	80.9		412	52.5	1.76	1730.1	82.3	1.68
278	55.7	1.82	1645.3	85.2		414	52.2	1.77	1731.0	79.9	1.74
280	55.5	1.85	1649.0	71.1		416	52.2	1.77	1733.2	68.1	1.60
282	54.2	1.87	1657.4	70.3		418	52.4	1.75	1734.7	63.4	1.59
284	53.1	1.82	1665.8	84.0		420	52.4	1.73	1736.4	73.2	1.61
286	51.9	1.80	1674.2	79.2		422	52.5	1.77	1738.1	65.0	1.70
288	49.9	1.80	1682.5	89.3		424	52.6	1.78	1739.7	71.6	1.67
290	50.4	1.81	1690.9	61.8		426	54.9	1.77	1721.5	71.2	1.64
292	53.4	1.82	1709.9	63.6		428	55.0	1.77	1703.9	72.0	1.83
294	52.1	1.76	1733.5	73.4		430	52.7	1.76	1736.9	62.8	1.78
296	51.5	1.75	1757.0	87.8		432	53.0	1.76	1724.3	65.3	1.72
298	52.2	1.76	1780.5	66.9		434	53.3	1.75	1723.2	68.6	1.66
300	52.9	1.76	1804.0	59.9		436	53.5	1.75	1722.1	80.0	1.67
302	53.7	1.76	1827.5	57.0		438	53.8	1.75	1720.9	58.0	1.79
304	54.5	1.75	1661.2	66.5		440	54.1	1.74	1719.8	68.0	1.78
306	54.7	1.79	1649.1	104.1		442	54.4	1.74	1718.7	52.0	1.74
308	54.3	1.80	1662.6	63.5		444	54.6	1.73	1717.5	65.3	1.77
310	55.0	1.74	1673.8	86.8		446	54.9	1.72	1716.4	63.6	1.41
312	55.0	1.68	1676.9	66.4		448	55.2	1.71	1715.3	62.1	1.78
314	53.0	1.66	1680.0	85.6		450	55.5	1.66	1714.2	55.0	1.83
316	54.7	1.75	1683.1	88.2		452	55.7	1.67	1713.0	67.6	1.76
318	58.3	1.81	1686.2	63.6		454	55.4	1.73	1718.4	67.0	1.80
320	60.3	1.76	1689.3	69.1		456	56.2	1.76	1722.3	68.3	1.83
322	59.6	1.78	1676.1	66.0		458	59.8	1.77	1658.7	67.9	1.76
324	55.1	1.78	1649.3	63.7		460	57.0	1.77	1664.2	65.4	1.80
326	52.8	1.75	1695.1	65.8		462	53.0	1.75	1697.8	60.7	1.73
328	52.3	1.73	1696.2	67.8		464	54.0	1.72	1752.3	66.2	1.69
330	52.8	1.70	1697.3	69.8		466	54.4	1.73	1746.5	79.8	1.70
332	54.2	1.76	1689.2	71.9		468	54.3	1.75	1740.7	67.1	1.66
334	55.9	1.81	1678.5	73.9		470	55.7	1.69	1701.7	61.6	1.70
336	57.7	1.82	1667.7	76.0		472	56.7	1.62	1645.4	65.6	1.70
338	59.5	1.80	1657.0	78.0		474	55.4	1.69	1624.3	63.9	1.70
340	53.7	1.78	1686.8	80.0		476	54.1	1.76	1653.8	68.6	1.81
342	53.1	1.76	1696.7	82.1		478	60.0	1.78	1683.3	61.2	1.73
344	52.7	1.76	1686.4	84.1		480	60.5	1.77	1712.8	62.2	1.71
346	53.4	1.77	1729.6	86.1		482	57.2	1.75	1730.4	66.5	1.75
348	54.0	1.78	1817.4	88.2		484	53.8	1.73	1716.2	61.9	1.67
350	54.6	1.78	1709.1	90.2		486	53.8	1.63	1721.3	60.6	1.70
352	54.3	1.78	1702.0	92.3		488	54.0	1.66	1704.4	54.6	1.64
354	53.8	1.79	1695.0	94.3		490	54.5	1.71	1709.7	63.6	1.59
356	53.4	1.79	1688.1	94.3	1.17	492	57.9	1.74	1713.2	77.3	1.69
358	53.2	1.77	1686.2	94.0	1.22	494	63.5	1.71	1716.1	63.8	1.77
360	52.7	1.74	1691.3	75.1	1.35	496	58.0	1.65	1712.0	63.5	1.66
362	51.7	1.72	1683.2	66.9	1.52	498	54.1	1.55	1707.9	67.3	1.73
364	51.8	1.74	1689.2	60.9	1.38	500	53.1	1.55	1703.8	62.6	1.66
366	53.6	1.73	1695.6	64.5	1.64	502	57.2	1.56	1699.7	64.9	1.68
368	54.6	1.68	1699.0	64.4	1.74	504	61.5	1.63	1696.3	64.2	1.78
370	54.7	1.65	1697.9	75.6	1.59	506	65.1	1.75	1686.0	72.3	1.82
372	54.6	1.64	1700.2	63.5	1.38	508	64.4	1.74	1686.3	74.5	1.70
374	55.7	1.62	1701.6	71.8	1.60	510	63.8	1.74	1673.2	65.0	1.73
376	57.3	1.61	1690.8	72.7	1.62	512	56.5	1.67	1681.0	64.9	1.66
378	58.2	1.63	1681.3	68.2	1.55	514	53.5	1.73	1738.5	64.8	1.66
380	59.1	1.68	1672.4	81.5	1.64	516	54.0	1.76	1722.9	67.1	1.67
382	60.0	1.63	1663.6	80.3	1.66	518	54.5	1.77	1718.1	53.5	1.62
384	60.9	1.67	1654.8	67.2	1.74	520	56.2	1.78	1736.8	65.1	1.64
386	57.8	1.72	1646.0	76.8	1.65	522	54.7	1.77	1743.5	67.5	1.65
388	60.1	1.76	1649.5	67.6	1.61	524	54.4	1.69	1676.2	65.7	1.73
390	61.3	1.76	1653.3	62.6	1.63	526	54.5	1.65	1682.8	54.5	1.72
392	59.0	1.75	1674.5	65.4	1.63	528	54.6	1.62	1689.4	66.0	1.64
394	56.8	1.75	1698.9	63.3	1.69	530	56.0	1.64	1695.9	68.7	1.73
396	54.8	1.78	1722.8	69.0	1.75	532	58.9	1.67	1717.3	63.9	1.76
398	54.8	1.79	1701.2	72.3	1.79	534	61.5	1.70	1734.5		1.76
400	55.1	1.79	1710.0	60.0	1.62	536	61.2	1.71	1730.5		1.74
402	54.8	1.80	1705.9	72.6	1.71	538	58.4	1.69	1716.1		1.78
404	54.0	1.80	1710.4	65.4	1.66	540	56.1	1.61	1717.6		1.82

Table T3 (continued).

Depth (mbsf)	Core log			Downhole log	
	Porosity (%)	Density (g/cm ³)	Velocity (m/s)	Porosity (%)	Density (g/cm ³)
542	54.1	1.56	1729.5		1.76
544	55.2	1.57	1716.7		1.72
546	58.3	1.69	1706.8		
548	63.5	1.76	1696.9		
550	64.1	1.76	1687.0		
552	61.8	1.77	1677.1		
554	55.4	1.77			
556	53.9	1.77			
558	53.7	1.78			
560	53.6	1.78			
562	53.4	1.77			
564	53.3	1.76			
566	53.1	1.76			
568	53.2	1.75			
570	54.0	1.75			
572	54.2	1.73			
574	54.4	1.59			
576	54.5				
578	55.0				
580	56.2				
582	58.9				
584	62.7				

Table T4. Core porosity, density, and velocity, Site 1101.

Depth (mbsf)	Porosity (%)	Density (g/cm ³)	Velocity (m/s)	Depth (mbsf)	Porosity (%)	Density (g/cm ³)	Velocity (m/s)
2	72.1	1.51	1528.0	110	60.5	1.73	1582.5
4	70.7	1.53	1533.6	112	57.2	1.80	1585.8
6	69.3	1.55	1538.7	114	51.0	1.88	1571.1
8	68.0	1.58	1537.3	116	44.8	1.95	1601.5
10	66.8	1.60	1553.2	118	45.7	1.95	1596.1
12	65.6	1.62	1651.1	120	52.0	1.88	1603.8
14	64.4	1.64	1534.4	122	50.2	1.88	1604.0
16	64.9	1.63	1537.8	124	58.5	1.74	1566.1
18	66.3	1.61	1541.8	126	61.7	1.68	1608.0
20	67.7	1.58	1552.0	128	59.1	1.73	1579.1
22	66.6	1.60	1553.6	130	58.7	1.71	1616.0
24	66.4	1.60	1532.8	132	52.4	1.83	1624.8
26	65.2	1.62	1566.2	134	60.5	1.70	1566.8
28	62.1	1.67	1556.0	136	53.1	1.82	1626.6
30	62.1	1.68	1549.7	138	53.8	1.83	1621.6
32	62.1	1.68	1543.4	140	54.1	1.82	1625.0
34	61.8	1.69	1560.3	142	54.1	1.82	1628.5
36	61.1	1.70	1573.2	144	54.1	1.81	1632.0
38	63.2	1.65	1570.6	146	54.6	1.80	1594.0
40	64.1	1.63	1567.2	148	57.2	1.76	1586.2
42	64.1	1.64	1563.8	150	57.3	1.75	1585.4
44	64.1	1.64	1560.4	152	56.3	1.77	1586.7
46	64.1	1.65	1557.0	154	55.5	1.79	1593.0
48	60.3	1.71	1553.6	156	55.3	1.80	1599.3
50	63.5	1.66	1607.2	158	56.6	1.77	1605.6
52	57.4	1.76	1587.0	160	54.8		1624.2
54	56.3	1.78	1574.2	162	57.2		1620.2
56	63.8	1.64	1580.1	164	59.6	1.70	1614.3
58	60.8	1.69	1587.7	166	58.1	1.73	1608.5
60	58.0	1.73	1570.4	168	56.6	1.76	1602.7
62	56.0	1.77	1596.7	170	55.1	1.80	1602.6
64	55.0	1.80	1600.0	172	55.7	1.78	1611.7
66	55.1	1.81	1567.6	174	56.4	1.76	1614.2
68	60.5	1.71	1564.0	176	57.1	1.75	1616.7
70	67.9	1.58	1569.8	178	60.5	1.68	1610.6
72	64.4	1.63	1565.3	180	62.1	1.65	1603.8
74	60.6	1.70	1582.1	182	62.0	1.66	1605.2
76	56.8	1.77	1588.5	184	61.3	1.66	1610.2
78	53.3	1.82	1607.9	186	59.8	1.69	1605.9
80	60.7	1.72	1591.5	188	57.5	1.74	1632.1
82	60.9	1.71	1570.7	190	59.2	1.71	1623.5
84	52.2	1.83	1579.7	192	61.9	1.65	1616.8
86	53.2	1.82	1607.7	194	62.1	1.66	1627.3
88	54.0	1.81	1596.0	196	60.6	1.68	1619.4
90	54.2	1.80	1570.6	198	57.5	1.71	1603.5
92	55.3	1.80	1589.1	200	50.8	1.70	1619.7
94	57.1	1.78	1628.3	202	50.6	1.70	1642.4
96	60.6	1.72	1564.8	204	58.9	1.69	1688.9
98	62.4	1.69	1567.7	206	59.5	1.69	1635.4
100	62.5	1.69	1572.5	208	60.7	1.67	1616.3
102	57.8	1.74	1568.1	210	65.6	1.60	1607.2
104	55.0	1.80	1615.0	212	64.6	1.62	1624.9
106	52.3	1.85	1606.5	214	63.0	1.65	1615.0
108	61.1	1.70	1566.5				

Table T5. Two-way traveltimes-depth relationship of main stratigraphic boundaries.

Stratigraphic boundary	Site 1095		Site 1096		Site 1101	
	Depth (mbsf)	TWT (ms)	Depth (mbsf)	TWT (ms)	Depth (mbsf)	TWT (ms)
Seismic stratigraphy*:						
M1/M2	90	110	323	400	190	240
M2/M3	182	220	618	741	338	420
M3/M4	505	580	950	1100	664	795
M4/M5	852	920	1290	1440	909	1060
M5/M6	1012	1060	1548	1680		
Basement	1431	1380	2154	2180	1166	1320
Lithostratigraphic unit						
I/II	49	60	63	82	53	68
II/III	436	506	173	219	143	181
III/Base	570	647	608	729	218	274

Notes: TWT = two-way traveltimes. * = after Rebesco et al, 1997. We used the second-order time-depth functions outlined in Figures [F11](#), p. 21, [F15](#), p. 26, and [F17](#), p. 27.